Transient mechanics of foams and emulsions

Boschan, J.

DOI
10.4233/uuid:7d2ced9a-1b58-40d1-9e2c-0e4fb6a1c882

Publication date
2021

Document Version
Final published version

Citation (APA)
Boschan, J. (2021). *Transient mechanics of foams and emulsions*. [Dissertation (TU Delft), Delft University of Technology]. https://doi.org/10.4233/uuid:7d2ced9a-1b58-40d1-9e2c-0e4fb6a1c882

Transient mechanics of foams and emulsions

Transient mechanics of foams and emulsions

Proefschrift

ter verkrijging van de graad van doctor
aan de Technische Universiteit Delft,
op gezag van de Rector Magnificus prof. ir. T.H.J.J. van der Hagen,
voorzitter van het College voor Promoties,
in het openbaar te verdedigen op maandag 18 januari 2021 om 10:00 uur

door

Júlia BOSCHÁN

Master of Science in Nuclear Engineering,
Eidgenössische Polytechnische Schule, Zürich, Zwitserland en
École polytechnique fédérale, Lausanne, Zwitserland,
geboren te Budapest, Hongarije.

Dit proefschrift is goedgekeurd door de

promotor:	Prof. dr. ir. T.J.H. Vlugt
copromotor:	Dr. B.P. Tighe

Samenstelling promotiecommissie:

Rector Magnificus,	voorzitter
Prof. dr. ir. T.J.H. Vlugt,	Technische Universiteit Delft
Dr. B.P. Tighe,	Technische Universiteit Delft
Onafhankelijke leden:	
Prof. dr. ir. J.T. Padding,	Technische Universiteit Delft
Prof. dr. D.J.E.M. Roekaerts,	Technische Universiteit Delft
Prof. dr. J.H. Snoeijer,	Universiteit Twente
Dr. T. Idema,	Technische Universiteit Delft
Dr. W. Ellenbroek,	Technische Universiteit Eindhoven

This work was sponsored by NWO Exacte Wetenschappen (Physical Sciences) for the use of supercomputer facilities, with financial support form the Nederlandse Organisatie voor Wetenschappelijk Onderzoek (Netherlands Organization for Scientific Research, NWO).

Keywords: Jamming, Rheology, Viscoelasticty, Plasticty, Marginal Solids, Soft Spheres, Shear Modulus

Printed by: Ridderprint BV | www.ridderprint.nl

Cover by: K. Fehrl

ISBN 978-94-6366-349-6

An electronic version of this dissertation is available at
http://repository.tudelft.nl/.

To my mother, Dr. Eva Borbas.

Contents

Summary ix

Samenvatting xi

1 Introduction 1
- 1.1 Jamming transition in foams . . . 3
- 1.2 Mechanics of jammed solids . . . 4
- 1.3 Simulations of jammed solids . . . 7
- 1.4 Structure of this thesis . . . 8

2 Beyond linear elasticity 11
- 2.1 Introduction . . . 12
- 2.2 Soft spheres: Model and background . . . 14
  - 2.2.1 Model . . . 14
  - 2.2.2 Shear modulus and the role of contact changes . . . 16
- 2.3 Stress relaxation . . . 18
  - 2.3.1 Scaling in the relaxation modulus . . . 19
- 2.4 Finite strain . . . 22
  - 2.4.1 Flow start-up . . . 23
  - 2.4.2 Quasistatic stress-strain curves . . . 23
  - 2.4.3 Onset of softening . . . 24
  - 2.4.4 Hertzian packings . . . 25
  - 2.4.5 Relating softening and contact changes . . . 25
  - 2.4.6 Rate-dependence . . . 28
- 2.5 Implications for experiment . . . 30
- 2.6 Discussion . . . 31

3 Stress Relaxation 35
- 3.1 Introduction . . . 36
- 3.2 Methods and Model . . . 38
- 3.3 Stress relaxation at finite strain . . . 39
- 3.4 Relaxation time and strain dependence . . . 40
- 3.5 Relaxation and non-affine particle motion . . . 42
- 3.6 Conclusion . . . 46

4 Jamming and Irreversibility 49
- 4.1 Model and Methods . . . 51
- 4.2 Plastic Work . . . 52
- 4.3 Contact changes . . . 54
  - 4.3.1 Contact changes during loading . . . 55

4.3.2 Contact changes after reversal 56
4.3.3 Relating nonlinearity and irreversibility 57
4.3.4 From contact changes to the stress-strain curve 58
4.4 Discussion 58

5 Conclusions and Outlook **61**

References **65**

Curriculum Vitæ **73**

List of Publications **75**

Acknowledgements **77**

Summary

Systems far from equilibrium have numerous practical uses, but challenge our understanding of their underlying physics. Materials like foams, emulsions, suspensions and granular matter can show liquid-like properties or get trapped in a solid-like jammed state. The phase transition between the flowing and static state is often referred to as the 'jamming transition'.

This work focuses on the mechanical behavior of amorphous viscoelastic materials, close to the jamming point. In many traditional solids, the relation between stress and strain is well described by a linear proportionality, known as Hooke's law. In jammed solids, by contrast, the stress-strain relation quickly becomes nonlinear, making them much harder to model. Here we ask how and why the linear response breaks. To answer the questions, we investigate the breakdown of linear response as a function of deformation rate and amplitude.

In Ch. 2 we map out the boundaries to Hooke's law by systematically performing stress relaxation and shear start up tests. We then derive scaling arguments, that define the window where linear response is valid. Our results show that the window vanishes at the transition, meaning that even small or slow deformations will break linear response.

In Ch. 3 we investigate the relation between viscoelasticty and nonlinear effects. The relaxation time is the governing time scale in the dynamics of viscoelastic materials. On comparatively short time scales viscous losses are dominant. On relatively long time scales the behavior of the material is determined mainly by elastic forces. By performing step strain experiments, we map out the dependence of the relaxation time on strain amplitude and the distance to jamming. We find two windows in strain where the relaxation time is insensitive to the strain amplitude, and determined only by the distance to jamming. Surprisingly, even the window at high strain is well described by theoretical predictions derived for vanishingly small strains.

In Ch. 4 we investigate connection between nonlinearity and irreversibility. By performing shear reversal tests, we observe plastic work as a function of the maximally applied strain and the distance to jamming. Remarkably, we find that even for small, linear deformations the plastic work is nonzero. This means that some degree of irreversibility is already present even when the stress-strain curve has not deviated from its linear elastic form. We find that irreversibility grows with strain and eventually saturates. From these observations we conclude, that irreversibility

precedes softening and that nonlinearity is connected only to a ‘fully developed‘ irreversibility.

Samenvatting

Systemen ver uit evenwicht hebben verschillende praktische toepassingen. Het is echter een uitdaging om het gedrag van deze systemen goed te begrijpen. Materialen zoals schuim, emulsies, suspensies en granulaire materialen kunnen eigenschappen hebben van vloeistoffen, maar ook van vaste stoffen. Dit laatste betreft de zogenaamde *jammed state*. De faseovergang tussen een vloeistofachtige fase en de *jammed state* wordt de jamming transitie genoemd.

Dit proefschrift beschrijft het mechanisch gedrag van amorfe visco-elastische materialen in de buurt van het jamming punt. Voor de meeste (conventionele) vaste stoffen wordt de relatie tussen spanning en vervorming beschreven door de wet van Hooke, die stelt dat vervorming en spanning recht evenredig met elkaar zijn. Voor systemen in de *jammed state* zijn vervorming en spanning niet evenredig. Dit maakt de modellering van mechanische eigenschappen een stuk lastiger. Graag willen we weten waarom er een niet-lineair verband bestaat tussen vervorming en spanning voor systemen in de *jammed state*. Om dit te begrijpen wordt onderzocht hoe de afwijking van dit lineaire verband samenhangt met de deformatiesnelheid en amplitude van de vervorming.

In hoofdstuk Ch. 2 onderzoeken we de limiet van de toepasbaarheid van de wet van Hooke door systematisch de initiële schuifspanning te variëren en de spanningsrelaxatie te meten. Dit leidt tot schalingsregels waarmee precies kan worden gedefinieerd waar lineaire respons geldig is en waar niet. De resultaten laten zien dat het gebied waar lineaire respons geldig is geheel verdwijnt in de buurt van het *jamming point*, zodat daar zelfs hele kleine of langzame deformaties niet voldoen aan de wet van Hooke.

De relatie tussen visco-elasticiteit en niet-lineaire effecten wordt onderzocht in hoofdstuk Ch. 3. De dynamica van visco-elastische materialen wordt bepaald door de relaxatietijd. Op korte tijdschalen zijn visceuze verliezen dominant. Op lange tijdschalen wordt het gedrag van materialen bepaald door elastische krachten. Door een stapvormige vervorming aan te brengen wordt de invloed van de amplitude van de vervorming en de afstand tot het *jamming point* op de relaxatietijd onderzocht. Er zijn twee gebieden in het domein van mogelijke vervormingen waarbij de relaxatietijd vrijwel onafhankelijk is van de amplitude van de vervorming. Tot onze verrassing wordt het gebied bij grote vervorming nauwkeurig beschreven door theoretische voorspellingen afgeleid voor zeer kleine vervormingen.

In hoofdstuk Ch. 4 wordt het verband tussen niet-lineariteit en irreversibiliteit onderzocht. Door het uitvoeren van omgekeerde afschuifproeven

wordt zogenaamd *plastic work* waargenomen als functie van de maximaal toegepaste vervorming en de afstand tot het *jamming point*. Verrassend genoeg blijkt dat zelfs voor kleine lineaire deformaties de *plastic work* niet gelijk is aan nul. Daaruit blijkt dat enige mate van irreversibiliteit reeds aanwezig is indien de spanning-vervormingscurve niet afwijkt van lineair gedrag. Deze irreversibiliteit neemt toe met toenemende vervorming en vlakt uiteindelijk af tot een plateauwaarde. Hieruit kan geconcludeerd worden dat irreversibiliteit voorafgaat aan het zacht worden van het materiaal, en dat niet-lineariteit alleen gerelateerd is aan een volledig ontwikkelde irreversibiliteit.

1

Introduction

1

What do shaving foam and sand on the beach have in common? If we hold the two materials in our hands, we might not observe many similarities. Nevertheless, they do share particular properties. For instance, both can behave like a liquid or solid, depending on the circumstances.

Figure 1.1: Sand flowing through an hourglass.

Sand, a granular material, flows through an hourglass and splashes to the bottom, in a way that is reminiscent of water flowing out of a faucet, visible in Fig. 1.1. However, it does not fill up the bottom as a conventional fluid would, but creates a solid pile. Shaving foam can also from a "pile" on your hand, but it flows when you smear it on your skin. Sand and foams have a comparable microscopic structure, from which follow similar properties. Sand is comprised of many individual grains, which are different shapes and sizes. As all grains are different they can only arrange in a disordered manner. Similarly, when observed under a microscope, shaving foam is comprised of individual, not grains, but bubbles dispersed in water. The bubbles are polydispersed and disordered like the sand, and only interact when they are almost or actually touching each other. Due to the different shapes and sizes of the grained and bubbles, it is impossible for them to arrange in a ordered, crystalline structure. Instead they jam into disordered solid-like states.

Aside from granular matter and foams, there exist other materials which also display a similar disordered liquid-solid transition. When emulsions for example are subjected to a high enough stress, they lose any kind of rigidness and start to flow. Think of face cream as it is taken out of container. It does not flow down your arms, but it is possible to smear it on your hands.

The threshold above which a material yields and flows is called the *yield stress*. The yield stress changes with the volume fraction, that is denser systems must overcome a larger threshold to flow.

We see that all these are very different materials, but nevertheless share similar properties. In [2], Liu and Nagel presented a phase diagram, combining observations about dense amorphous matter. (A third axis temperature is omitted because this thesis deals only with non-Brownian systems.) We only consider two principal axes of the phase diagram, the stress σ and the volume fraction ϕ, shown in Fig. 1.2. We see the boundary between jammed and unjammed phases. Jammed amorphous lose their rigidity through decreasing volume fraction or yielding. Point J in

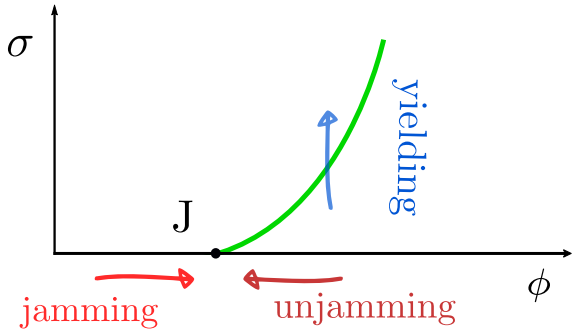

Figure 1.2: The jamming phase diagram. Arrow icon by [1]

this sense is quite remarkable. A material with zero stress can, at one point, cross over to the unjammed phase. That means that at point J, we can speak of a critical volume fraction $\phi(J) = \phi_c$. Materials in this state are marginally stable [3].

1.1. Jamming transition in foams

Point J corresponds to the state where the volume fraction, equals that of a random close packing. The random close packing volume fraction is the highest that randomly assembled particles can occupy while the external pressure is zero. In three dimensions it is $\phi_c^{3D} = 64\%$ and in two dimensions it is $\phi_c^{2D} = 84\%$ [4–6]. If the volume fraction is increased above RCP, by applying pressure, the material jams, and can act as a solid.

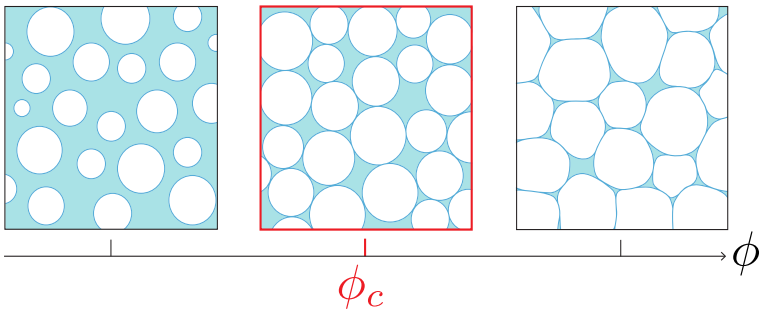

Figure 1.3: Schematic of a foam as the volume fraction changes, highlighting the specially of the jamming transition at ϕ_c

Fig. 1.3 illustrates the microscopic changes in a foam while the volume fraction increases and crosses the critical point. At low ϕ bubbles have enough space to spread out and do not touch. Because the bubble interactions are short ranged and repulsive [7], the individual bubbles are unaware of each other. The material properties are then dominated by the continuous phase, exhibiting liquid-like behavior. At the critical

point, $\phi = \phi_c$, the bubbles suddenly start touching. Upon contact, they exert repulsive force on each other, because surface tension favors spherical shapes.

Because the bubbles repel one another, contact is only possible when they are confined by an external stress due to e.g walls or gravity. At ϕ_c an entire contact network is formed, spanning through the whole system. The bubbles jam, and the material becomes rigid [8] i.e. it is capable of resisting bulk changes to its size and/or shape. The average number of contacts, z, is zero below critical volume fraction and jumps form zero to a finite number, at ϕ_c [4].

What is the minimum average number of contacts per bubble, that is needed in order for the material to jam? In [9], Maxwell introduced a counting argument which balances degrees of freedom (particle positions) and constraints (the contacts). The result is that the average number of contacts at the critical point z_c must be

$$z_c = 2d, \tag{1.1}$$

where d is the number of spatial dimensions. A system in which $z = z_c$ is termed isostatic. Point-J is an isostatic point [4, 10], where the number of contacts are just enough for the material to be rigid. Hence the distance to isostaticty $\Delta z = z - z_c$ is also a useful quantifier of the system's state.

1.2. Mechanics of jammed solids

As foams and emulsions are soft, they can be pushed above the jamming volume fraction. Then bubbles are pressed into each other, abandoning their spherical shape as shown in Fig. 1.3. By compressing them, the number of contacts increases. Because of this contact network, the amorphous solid can support stress. Earlier works establish [4, 7, 11] a scaling argument for the average number of contacts per particle that the system has in excess of z_c

$$z - z_c \sim (\phi - \phi_c)^{1/2}. \tag{1.2}$$

The pressure also changes as the volume fraction increases. At ϕ_c bubbles touch without deforming, and so

$$p_c = 0. \tag{1.3}$$

Above ϕ_c bubbles deform, leading to a pressure that grows linearly with the excess volume fraction [4],

$$p - p_c \sim p \sim \phi - \phi_c. \tag{1.4}$$

Where convenient, we will use p as a measure of distance to (un)jamming.

In conventional solids, when deformations are small the stress response is linear, meaning if the strain is doubled the stress also doubles.

However, if the deformation is reversed the material returns to its original form. The linear approximation is mathematically simple and universally applicable for small enough deformations. *Hooke's law* [12, 13] expresses the linear relation of strain γ and stress σ,

$$\sigma = G\gamma, \tag{1.5}$$

where G is the shear modulus, a material property. In jammed solids the shear modulus depends the distance to hamming and vanishes at ϕ_c,

$$G \sim \phi - \phi_c{}^{1/2}, \tag{1.6}$$

as illustrated in Fig. 1.4 [4, 14].

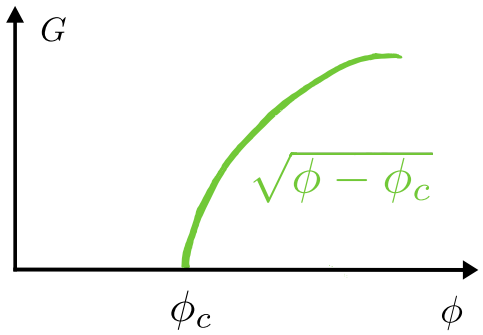

Figure 1.4: Evolution of the shear modulus as a function of the volume fraction.

In many conventional solids, Hooke's law gives a good description of the stress-strain curve up the point where they fail. Amorphous solids, on the other hand, can easily be pushed into the regime where Hooke's law is violated. There are two main ways, Hooke's law can break - either the deformation is too fast or too large. We describe these in turn.

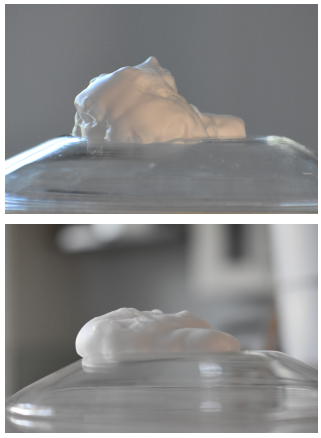

Figure 1.5: Collapsing of shaving foam in time. (top) fresh foam, (bottom) decaying in time.

Viscoelaticty Taking some shaving foam out of a can and simply putting it on a surface, it will sit on it and keep its form, like in the top picture in Fig. 1.5. This is a hallmark of a solid. After some time has passed the foam will lose its shape and start to collapse, as seen in the bottom picture in Fig. 1.5 [15, 16]. When bubbles slide past each other, they dissipate energy. This dissipation is viscous, i.e. it depends on the rate of deformation. Viscous dissipation is neglected in Hooke's law, which depends on

strain but not on strain rate. If the system is sheared slowly enough, viscous effects can indeed be neglected. For higher strain rates, however, viscous contributions to the stress become comparable to elastic contributions, and can no longer be neglected. The competition between elastic storage and viscous losses is governed by a characteristic time scale, the relaxation time. A deformation is "fast" if the inverse strain rate is smaller than the relaxation time. One of the main results of this thesis will be to show that, close to the jamming transition, viscous effects grow in importance and cannot be neglected.

Fig. 1.6 illustrates the process of relaxation in a jammed solid [17]. The particles are initially displaced according to an affine profile (Fig. 1.6a). However, these new positions are not force balanced. The particles then move non-affinely until mechanical equilibrium is reached. These non-affine motions are a significant source of dissipation.

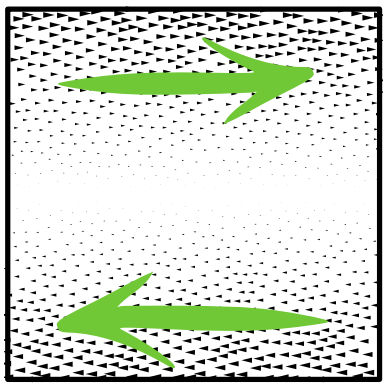

(a) Affine displacement of particles.

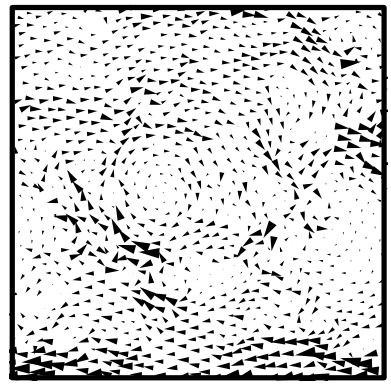

(b) Final displacement of individual particles, after returning to an equilibrium state.

Figure 1.6: Displacement of particles on a two dimensional system as a response to an affine displacement. Large arrow icon by [18]

Softening Small shear strains are reversible, meaning the system returns to its original state when an applied load is removed. But as strain builds up and the particles undergo rearrangements, it eventually happens that the system can no longer return to its initial state. The deformation is then said to be a mixture of elastic and plastic. One could assume that the onset of plasticity coincides with the "yield strain", i.e., the strain where $\sigma = \sigma_Y$. More generally, there is some strain $\gamma^\dagger$, where a system no longer follows the linear trend of Hooke's law, even if the strain rate is small to remove viscous effects. We call this softening. In Ch. 2 we show that in jammed matter, $\gamma^\dagger$ is much smaller then the yield strain, and even vanishes at ϕ_c.

1.3. Simulations of jammed solids

The results in this thesis are made based on extensive numerical simulations. All simulations are done using Durian's 'Bubble Model' [7, 19].

Bubble Model The model takes into account the forces acting on the bubbles when they touch. Upon contact real bubbles flatten out at the contact and increase the surface area of the gas-liquid interface. For simplicity, in the bubble model, the bubbles retain their spherical shape and the contact is characterized by comparing the sum of the radii, $R_i + R_j$ of bubbles i and j to their center-to-center distance r_{ij}. The difference is the overlap between two bubbles, denoted by $\delta_{ij} = (R_i + R_j) - r_{ij}$.

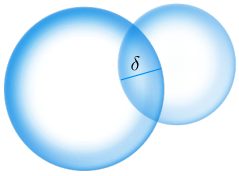

Figure 1.7: Illustration of bubble interaction in the Durian bubble model

The force between two bubbles is expressed as a function of the overlap,

$$\mathrm{f}_{ij}^{\mathrm{el}} = \begin{cases} k\delta\frac{\mathrm{r}_{ij}}{r_{ij}}, & \text{if } \delta < 0 \\ 0, & \text{otherwise,} \end{cases} \tag{1.7}$$

where k is the *spring constant*, which is proportional to the surface tension.

Energy is dissipated by the viscous force, which is proportional to the relative velocity $\mathrm{v}_{ij} = \mathrm{v}_j - \mathrm{v}_i$ of bubbles i and j.

$$\mathrm{f}_{ij}^{\mathrm{vis}} = \begin{cases} -b\mathrm{v}_{ij}, & \text{if } \delta < 0 \\ 0, & \text{otherwise,} \end{cases} \tag{1.8}$$

where b is a damping coefficient, proportional to the viscosity of the continuous phase. We choose units of stress and time such that the spring constant k and the damping coefficient b are both equal to one. As initial conditions packings with a fixed number of bubbles, at a fixed distance to jamming are created. The packings are bidisperse with a ratio of 1:1.4 in a 50:50 distribution [6]. Bubbles are placed randomly into a fixed volume. We then use an energy minimization algorithm (see below) to find a local energy minimum, where the gradients with respect to all particle degrees of freedom vanish, and the gradient with respect to the shear strain is

zero. The latter condition guarantees zero shear stress. When deforming the packings Lees-Edwards boundary conditions are applied [20].

Two types of simulations were used, molecular dynamics and quasistatic simulations. These have complementary strengths and weaknesses.

Molecular Dynamics (MD) Simulations This is an efficient method to resolve the dynamics of classical many body systems [21]. After each step, the particles move according to Newton's laws, which we integrate using the velocity Verlet algorithm. This simulation method allows to describe the time dependent dynamics of the problem. It places a high demand on computational power, compared to quasistatic methods. The time simulations take depends on the system size, N, the distance to the critical point (the pressure p) and the size of the deformation (strain step γ). Results are always ensemble averaged. For MD simulations we typically used an ensemble size of 100 packings. For a typical stress relaxation simulations we found that a system of $N = 1024$ particles can be simulated in a reasonable time frame for p as low as 10^{-5} and for strain step sizes $\gamma = 10^{-6} ... 10^{-2}$ (these are dimensionless parameters).

Quasistatic Simulations Because MD simulations are computationally costly, and for some measurements we are not specifically interested in the dynamics of the system, we also use quasistatic simulations. Quasistatic methods are appropriate for describing the response to deformations at arbitrarily slow rates. In this limit the system always sits at a local minimum, which depends on the particle positions and the shear strain. Applying a strain perturbs the landscape, causing the particles to move to a new minimum. This can be found using minimization routines such as nonlinear gradient method [5, 6] or FIRE [22]. Quasistatic simulations typically take a fraction of the time of MD simulations, which we exploit to generate higher ensembles. For our simulations the ensemble size is typically between 300-600.

1.4. Structure of this thesis

The work in this thesis is focused on the behavior of amorphous viscoelastic materials close to unjamming. We want to understand when and how the stress-strain response becomes nonlinear and/or rate dependent.

In Ch. 2 we investigate the limits of linear stress-strain response in soft sphere packings. Linear approximations are often used in simulations and experiments. We have mapped out the boundaries to Hooke's law by systematically performing stress relaxation and shear start up tests.

From these we derive scaling arguments that define the window where linear response is valid. Our results show that the window vanishes at the transition, meaning that even small or slow deformation will break linear response.

In Ch. 3 we investigate the relation between viscoelasticty and nonlinear effects. The relaxation time τ^* is the governing time scale in the dynamics of viscoelastic materials. Deformations slower than τ^* are governed by viscous forces, while for faster deformations they are negligible. We perform step strain tests to measure the relaxation time at varying step size. At low strains, in the linear regime the relaxation time is constant and increases when the response becomes nonlinear. Our results show that the relaxation time turns constant again for sufficiently high strains, i.e., the increase in the nonlinear regime is a crossover between two plateau values. This particular strain dependency scales with the distance to jamming. These results are important for interpreting experimental data near unjamming.

In Ch. 4 we investigate the connection between nonlinearity and irreversibility in soft sphere packings, to gain insight into the mechanics of softening. We perform shear reversal tests and compare the initial and final states of the packing. From these simulations we draw conclusions about macroscopic quantities, like plastic work and the underling microscopic topology of the system. Even after small linear deformations we find nonzero plastic work. The amount of plastic work increases as the maximum applied strain is increased. However, our results clearly show, that after a certain strain irreversibility saturates. Together with the macroscopic results we draw the conclusion, that irreversibility precedes softening, and that nonlinearity is connected only to a ‘fully developed‘ irreversibility.

2

Beyond linear elasticity

The shear response of soft solids can be modeled with linear elasticity, provided the forcing is slow and weak. Both of these approximations must break down when the material loses rigidity, such as in foams and emulsions at their (un)jamming point – suggesting that the window of linear elastic response near jamming is exceedingly narrow. Yet precisely when and how this breakdown occurs remains unclear. To answer these questions, we perform computer simulations of stress relaxation and shear start-up tests in athermal soft sphere packings, the canonical model for jamming. By systematically varying the strain amplitude, strain rate, distance to jamming, and system size, we identify characteristic strain and time scales that quantify how and when the window of linear elasticity closes, and relate these scales to changes in the microscopic contact network.

This chapter is based on the following publication: J. Boschan, D. Vågberg, E. Somfai, B.P. Tighe, Beyond linear elasticity: jammed solids at finite shear strain and rate , Soft Matter, 12, 5450-5460 (2016).

2.1. Introduction

Linear elasticity predicts that when an isotropic solid is sheared, the resulting stress σ is directly proportional to the strain γ and independent of the strain rate $\dot{\gamma}$,

$$\sigma = G_0\gamma\,, \tag{2.1}$$

with a constant shear modulus G_0.[12] The constitutive relation (2.1) – a special case of Hooke's law – is a simple, powerful, and widely used model of mechanical response in solids. Yet formally it applies only in the limit of vanishingly slow and weak deformations. In practice materials possess characteristic strain and time scales that define a linear elastic "window", i.e. a parameter range wherein Hooke's law is accurate. Determining the size of this window is especially important in soft solids, where viscous damping and nonlinearity play important roles.[23] The goal of the present work is to determine when Hooke's law holds, and what eventually replaces it, in soft sphere packings close to the (un)jamming transition.

Jammed sphere packings are a widely studied model of emulsions and liquid foams [7, 24–26] and have close connections to granular media and dense suspensions. [27–29] Linear elastic properties of jammed solids, such as moduli and the vibrational density of states, are by now well understood.[30, 31] Much less is known about their viscoelastic [27, 32] and especially their nonlinear response.[33, 34] Yet the jamming transition must determine the linear elastic window, because the shear modulus G_0 vanishes continuously at the jamming point, where the confining pressure p goes to zero. Indeed, studies of oscillatory rheology [35] and shocks [36–38] have shown that, precisely at the jamming point, *any* deformation is effectively fast and strong, and neither viscous effects nor nonlinearities can be neglected.

Because elasticity in foams, emulsions, and other amorphous materials results from repulsive contact forces, microstructural rearrangements of the contact network have signatures in the mechanical response. Namely, they lead to nonlinearity and irreversibility in the particle trajectories, and eventually to steady plastic flow.[39–44] Jammed packings of perfectly rigid particles cannot deform without opening contacts; their response is intrinsically nonlinear, and the number of contact changes per unit strain diverges in the limit of large system size.[45, 46] Recently Schreck and co-workers addressed contact changes inside the jammed phase[47–50]; specifically, they asked how many contact changes a jammed packing undergoes before linear response breaks down. They found that trajectories cease to be linear as soon as there is a single rearrangement (made or broken contact) in the contact network, and contact changes occur for vanishing perturbation amplitudes in large systems. Their findings caused the authors to question, if not the formal validity, then at least the usefulness of linear elasticity in jammed solids – not just at the jamming point, but anywhere in the jammed phase.

There is, however, substantial evidence that it is useful to distinguish between linear response in a strict sense, wherein particle trajectories follow from linearizing the equations of motion about an initial condition, and linear response in a weak sense, wherein the stress-strain curve obeys Hooke's law.[51–54] Hooke's law remains applicable close to but above jamming because coarse grained properties are less sensitive to contact changes than are individual trajectories. Agnolin and Roux verified numerically that linearization captures the initial slope of a stress-strain curve, while Van Deen et al. showed explicitly that the slope of the stress-strain curve is on average the same before and after the first contact change [51, 52]. Goodrich et al. further demonstrated that contact changes have negligible effect on the density of states.[54] These results verify the intuitive expectation that weak linear response remains valid even after strict linear response is violated. This in turn raises – but does not answer – the question of when Hooke's law eventually does break down.

Recent experiments [33, 41], simulations, [34, 44, 55, 56] and theory [57] provide evidence for a two stage yielding process, where response first becomes nonlinear (stress is no longer directly proportional to strain) and only later establishes steady plastic flow (stress is independent of strain). To distinguish these two crossovers, we will refer to them as softening and yielding, respectively; our focus will be mainly on the softening crossover. It remains unclear precisely how rate dependence, nonlinearity, and contact changes contribute to the breakdown of linear elasticity and onset of softening. In order to unravel these effects, it is necessary to vary strain, strain rate, pressure, and system size simultaneously and systematically – as we do here for the first time. Using simulations of viscous soft spheres, we find that Hooke's law is valid within a surprisingly narrow window bounded by viscous dissipation at small strain and plastic dissipation at large strain. The size of the linear elastic window displays power law scaling with pressure and correlates with the accumulation of not one, but an extensive number of contact changes.

The basic scenario we identify is illustrated in Fig. 2.1, which presents ensemble-averaged shear stress versus strain. Shear is applied via a constant strain rate $\dot{\gamma}_0$ at fixed volume. We identify three characteristic scales, each of which depend on the initial pressure p: (i) For strains below $\gamma^* \equiv \dot{\gamma}_0 \tau^*$, where τ^* is a diverging time scale, viscous stresses are significant and Eq. (2.1) underestimates the stress needed to deform the material. This crossover strain vanishes under quasistatic shear ($\dot{\gamma}_0 \to 0$, filled squares). (ii) Above a vanishing strain $\gamma^\dagger$ the material softens and Hooke's law overestimates the stress. This crossover is rate-independent, consistent with plastic effects. (iii) For strain rates above a vanishing scale $\dot{\gamma}^\dagger$ (triangles), Eq. (2.1) is never accurate and there is no strain interval wherein the material responds as a linear elastic solid.

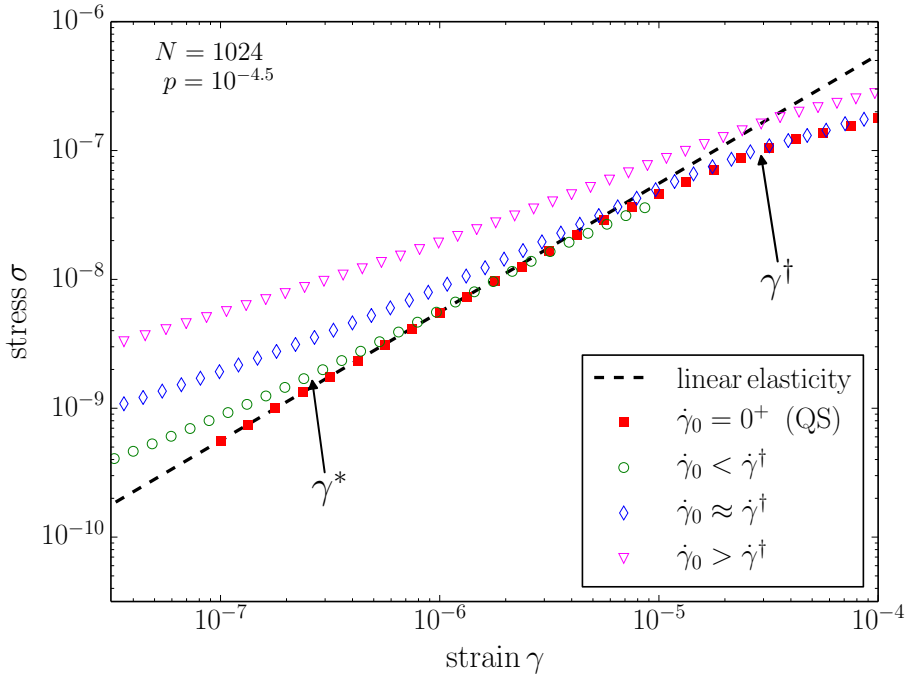

Figure 2.1: Ensemble-averaged stress-strain curves of packings sheared at varying strain rate $\dot\gamma_0$. Close to the jamming point the linear stress-strain curve (dashed line) predicted by Hooke's law holds over a narrow interval at low strain, with deviations due to viscous and plastic dissipation. The crossover strains γ^* and $\gamma^\dagger$ are indicated for the data sheared at slow but finite rate $0 < \dot\gamma_0 < \dot\gamma^\dagger$ (open circles).

2.2. Soft spheres: Model and background

We first introduce the soft sphere model and summarize prior results regarding linear elasticity near jamming.

2.2.1. Model

We perform numerical simulations of the Durian bubble model [7], a mesoscopic model for wet foams and emulsions. The model treats bubbles/ droplets as non-Brownian disks that interact via elastic and viscous forces when they overlap. Elastic forces are expressed in terms of the overlap $\delta_{ij} = 1 - r_{ij}/(R_i + R_j)$, where R_i and R_j denote radii and $\vec{r}_{ij}$ points from the center of particle i to the center of j. The force is repulsive and acts along the unit vector $\hat{r}_{ij} = \vec{r}_{ij}/r_{ij}$:

$$\vec{f}_{ij}^{\,\mathrm{el}} = \begin{cases} -k(\delta_{ij})\,\delta_{ij}\,\hat{r}_{ij}\,, & \delta_{ij} > 0 \\ \vec{0}, & \delta_{ij} < 0. \end{cases} \tag{2.2}$$

The prefactor k is the contact stiffness, which generally depends on the overlap

$$k = k_0\, \delta^{\alpha-2}\,. \tag{2.3}$$

Here k_0 is a constant and α is an exponent parameterizing the interaction. In the following we consider harmonic interactions ($\alpha = 2$), which provide a reasonable model for bubbles and droplets that resist deformation due to surface tension; we also treat Hertzian interactions ($\alpha = 5/2$), which correspond to elastic spheres.

We perform simulations using two separate numerical methods. The first is a molecular dynamics (MD) algorithm that implements SLLOD dynamics [58] using the velocity-Verlet scheme. Energy is dissipated by viscous forces that are proportional to the relative velocity $\Delta\vec{v}_{ij}^{\,c}$ of neighboring particles evaluated at the contact,

$$\vec{f}_{ij}^{\,\text{visc}} = -\tau_0\, k(\delta_{ij})\, \Delta\vec{v}_{ij}^{\,c}\,, \tag{2.4}$$

where τ_0 is a microscopic relaxation time. Viscous forces can apply torques, hence particles are allowed to rotate as well as translate.

In addition to MD, we also perform simulations using a nonlinear conjugate gradient (CG) routine [5], which keeps the system at a local minimum of the potential energy landscape, which itself changes as the system undergoes shearing. The dynamics are therefore quasistatic, i.e. the particle trajectories correspond to the limit of vanishing strain rate.

All results are reported in units where k_0, τ_0, and the average particle diameter have all been set to one. Each disk is assigned a uniform mass $m_i = \pi R_i^2$, which places our results in the overdamped limit.

Bubble packings consist of $N = 128$ to 2048 disks in the widely studied 50:50 bidisperse mixture with a 1.4:1 diameter ratio.[6] Shear is implemented via Lees-Edwards "sliding brick" boundary conditions at fixed volume V (area in two dimensions). The stress tensor is given by

$$\sigma_{\alpha\beta} = \frac{1}{2V}\sum_{ij} f_{ij,\alpha} r_{ij,\beta} - \frac{1}{V}\sum_{i} m_i v_{i,\alpha} v_{i,\beta}\,, \tag{2.5}$$

where $\vec{f}_{ij}$ is the sum of elastic and viscous contact forces acting on particle i due to particle j, and $\vec{v}_i$ is the velocity of particle i. Greek indices label components along the Cartesian coordinates x and y. The confining pressure is $p = -(1/D)(\sigma_{xx} + \sigma_{yy})$, where $D = 2$ is the spatial dimension, while the shear stress is $\sigma = \sigma_{xy}$. The second term on the righthand side of Eq. (2.5) is a kinetic stress, which is always negligible in the parameter ranges investigated here.

We use the pressure p to measure a packing's distance to jamming. Common alternatives are the excess volume fraction $\Delta\phi = \phi - \phi_c$ and excess mean contact number $\Delta z = z - z_c$, where ϕ_c and $z_c = 2D$ refer to the respective values at jamming.[4, 30, 59] We prefer to use the pressure as an order parameter because it is easily accessed in experiments (unlike z),

and its value at the transition, $p_c = 0$, is known exactly (unlike ϕ). Therefore, prior to shearing, all packings are prepared at a targeted pressure. The equilibration procedure includes the box size and shape in addition to the particle positions as degrees of freedom, which guarantees that the stress tensor is proportional to the unit matrix and that the packing is stable to shear perturbations.[60] At each pressure there are fluctuations in ϕ and z, however for a given preparation protocol the probability distributions of ϕ and z tend to a delta function with increasing N [4, 5], and typical values (e.g. the mean or mode) satisfy the scaling relation

$$\frac{p}{k} \sim \Delta\phi \sim \Delta z^2 \,. \tag{2.6}$$

Here k is a typical value of the contact stiffness $k(\delta_{ij})$ in Eq. (2.3), which is simply the constant k_0 in the harmonic case ($\alpha = 2$). For other values of α, however, k depends on the pressure. As the typical force trivially reflects its bulk counterpart, $f \sim p$, the contact stiffness scales as $k \sim f/\delta \sim p^{(\alpha-2)/(\alpha-1)}$. In the following, all scaling relations will specify their dependence on k and the time scale τ_0. In the present work τ_0 is independent of the overlap between particles (as in the viscoelastic Hertzian contact problem [61]), but we include τ_0 because one could imagine a damping coefficient $k\tau_0$ with more general overlap dependence than the form treated here.

2.2.2. Shear modulus and the role of contact changes

In large systems the linear elastic shear modulus G_0 vanishes continuously with pressure,

$$G_0/k \sim (p/k)^{\mu} \,, \tag{2.7}$$

with $\mu = 1/2$. Hence jammed solids' shear stiffness can be arbitrarily weak. The scaling of G_0 has been determined multiple times, both numerically [4, 62, 63] and theoretically [14, 35, 64]; it is verified for our own packings in Fig. 2.3a and c, as discussed in Section 2.3.

There are two standard approaches to determining G_0. The first, which we employ, is to numerically impose a small but finite shear strain and relax the packing to its new energy minimum.[4, 62] In the second approach one writes down the D equations of motion for each particle and linearizes them about a reference state, which results in a matrix equation involving the Hessian; solutions to this equation describe the response to an infinitesimally weak shear.[3, 35, 60, 63–65] The latter approach allows access to the zero strain limit, but it is blind to any influence of contact changes.

When calculating the shear modulus using the finite difference method over strain differences as small as 10^{-9}, double precision arithmetic does not provide sufficiently accurate results.[66] A straightforward but computationally expensive approach is to switch to quadruple precision. Instead we represent each particle position as the sum of two double preci-

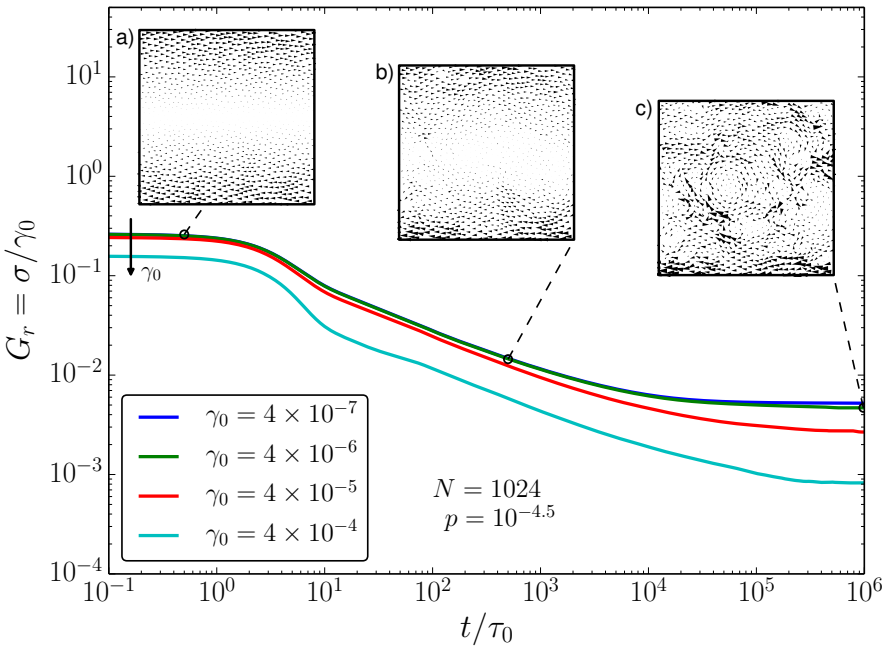

Figure 2.2: The ensemble-averaged relaxation modulus G_r at pressure $p = 10^{-4.5}$ for four values of the strain amplitude γ_0. In all four cases, G_r displays an initial plateau corresponding to affine particle motion (inset a), followed by a power law decay as the particle displacements become increasingly non-affine (b). At long times the stress is fully relaxed and the final particle displacements are strongly non-affine (c).

sion variables, which gives sufficient precision for the present work and is significantly faster than the GCC Quad-Precision Math Library. Since we are aware of precision issues, we have taken great care to verify our results. The shear modulus calculated using finite difference method agrees with the corresponding shear modulus obtained using the Hessian matrix [30], provided the strain amplitude is small enough that the packing neither forms new contacts, nor breaks existing ones.

Van Deen et al. [52] measured the typical strain at the first contact change, and found that it depends on both pressure and system size,

$$\gamma_{\mathrm{cc}}^{(1)} \sim \frac{(p/k)^{1/2}}{N} \,. \tag{2.8}$$

The inverse N-dependence is consistent with what one would expect from a Poisson process. Similar to the findings of Schreck et al. [47], who determined a critical perturbation amplitude by deforming packings along normal modes, the strain scale in Eq. (2.8) vanishes in the large system limit, even at finite pressure. Earlier work by Combe and Roux probed

deformations of rigid disks precisely at jamming; they identified a dimensionless stress scale $\sigma_{cc}^{(1)}/p \sim 1/N^{1.16}$. Naïvely extrapolating to soft spheres would then give a strain scale $\gamma_{cc}^{(1)} \sim \sigma_{cc}^{(1)}/G_0 \sim (p/k)^{1/2}/N^{1.16}$, in reasonable but not exact agreement with Eq. (2.8).

2.3. Stress relaxation

We will characterize mechanical response in jammed solids using stress relaxation and flow start-up tests, two standard rheological tests. In the linear regime they are equivalent to each other and to other common tests such as creep response and oscillatory rheology, because complete knowledge of the results of one test permits calculation of the others.[23]

We employ stress relaxation tests to access the time scale τ^* over which viscous effects are significant, and we use flow start-up tests to determine the strain scale $\gamma^\dagger$ beyond which the stress-strain curve becomes nonlinear. We consider stress relaxation first.

In a stress relaxation test one measures the time-dependent stress $\sigma(t, \gamma_0)$ that develops in a response to a sudden shear strain with amplitude γ_0, i.e.

$$\gamma(t) = \begin{cases} 0 & t < 0 \\ \gamma_0 & t \geq 0\,. \end{cases} \tag{2.9}$$

The relaxation modulus is

$$G_r(t, \gamma_0) \equiv \frac{\sigma(t, \gamma_0)}{\gamma_0}\,. \tag{2.10}$$

We determine G_r by employing the shear protocol of Hatano.[27] A packing's particles and simulation cell are affinely displaced in accordance with a simple shear with amplitude γ_0. E.g. for a simple shear in the $\hat{x}$-direction, the position of a particle i initially at (x_i, y_i) instantaneously becomes $(x_i + \gamma_0 y_i, y_i)$, while the Lees-Edwards boundary conditions are shifted by $\hat{\gamma}_0 L_y$, where L_y is the height of the simulation cell. Then the particles are allowed to relax to a new mechanical equilibrium while the Lees-Edwards offset is held fixed.

The main panel of Fig. 2.2 illustrates four relaxation moduli of a single packing equilibrated at pressure $p = 10^{-4.5}$ and then sheared with strain amplitudes varying over three decades. All four undergo a relaxation from an initial plateau at short times to a final, lower plateau at long times. The character of the particle motions changes as relaxation progresses in time. While the particle motions immediately after the deformation are affine (Fig. 2.2a), they become increasingly non-affine as the stresses relax to a new static equilibrium (Fig. 2.2b,c).

For sufficiently small strain amplitudes, linear response is obtained and any dependence of the relaxation modulus on γ_0 is sub-dominant. The near-perfect overlap of the moduli for the two smaller strain amplitudes Fig. 2.2 indicates that they reside in the linear regime. The long-

time plateau is then equal to the linear elastic modulus G_0. In practice there is a crossover time scale τ^* such that for longer times $t \gg \tau^*$ viscous damping is negligible and the relaxation modulus is well approximated by its asymptote, $G_r \simeq G_0$. For the data in Fig. 2.2a the crossover time is $\tau^* \approx 10^4 \tau_0$. In the following Section we will determine the scaling of τ^* with pressure.

2.3.1. Scaling in the relaxation modulus

We now characterize stress relaxation in linear response by measuring the relaxation modulus, averaged over ensembles of packings prepared at varying pressure. We will show that G_r collapses to a critical scaling function governed by the distance to the jamming point, thereby providing a numerical test of recent theoretical predictions by Tighe.[35] In particular we test the prediction that the rescaled shear modulus G/G_0 collapses to a master curve when plotted versus the rescaled time t/τ^*, with a relaxation time that diverges as

$$\tau^* \sim \left(\frac{k}{p}\right)^{\lambda} \tau_0 \tag{2.11}$$

for $\lambda = 1$. Both the form of the master curve and the divergence of the relaxation time can be related to slowly relaxing eigenmodes that become increasingly abundant on approach to jamming. These modes favor sliding motion between contacting particles [63], reminiscent of zero energy floppy modes [67], and play an important role in theoretical descriptions of mechanical response near jamming.[3, 14, 35, 64, 68] For further details, we direct the reader to Ref. [35].

We showed in Fig. 2.2 that a packing relaxes in three stages. The short-time plateau is trivial, in the sense that viscous forces prevent the particles from relaxing at rates faster than $1/\tau_0$; hence particles have not had time to depart significantly from the imposed affine deformation and the relaxation modulus reflects the contact stiffness, $G_r \sim k$. We therefore focus hereafter on the response on time scales $t \gg \tau_0$.

To demonstrate dynamic critical scaling in G_r, we first determine the scaling of its long-time asymptote G_0. We then identify the time scale τ^* on which G_r significantly deviates from G_0. Finally, we show that rescaling with these two parameters collapses the relaxation moduli for a range of pressures to a single master curve. While we address variations with strain in subsequent Sections, the strain amplitude here is fixed to a value $\gamma_0 = 10^{-5.5}$. We have verified that this strain amplitude is in the linear regime for all of the data presented in this Section.

As noted above, at long times the relaxation modulus approaches the linear quasistatic modulus, $G_r(t \to \infty) \simeq G_0$. We verify Eq. (2.7) in our harmonic packings with two closely related tests. First we fit a power law to data from systems of $N = 2048$ particles; the best fit has a slope of 0.48 (Fig. 2.3a, dashed line). Next, we repeat the finite size scaling analysis of Goodrich et al. [69], who showed that finite size effects become

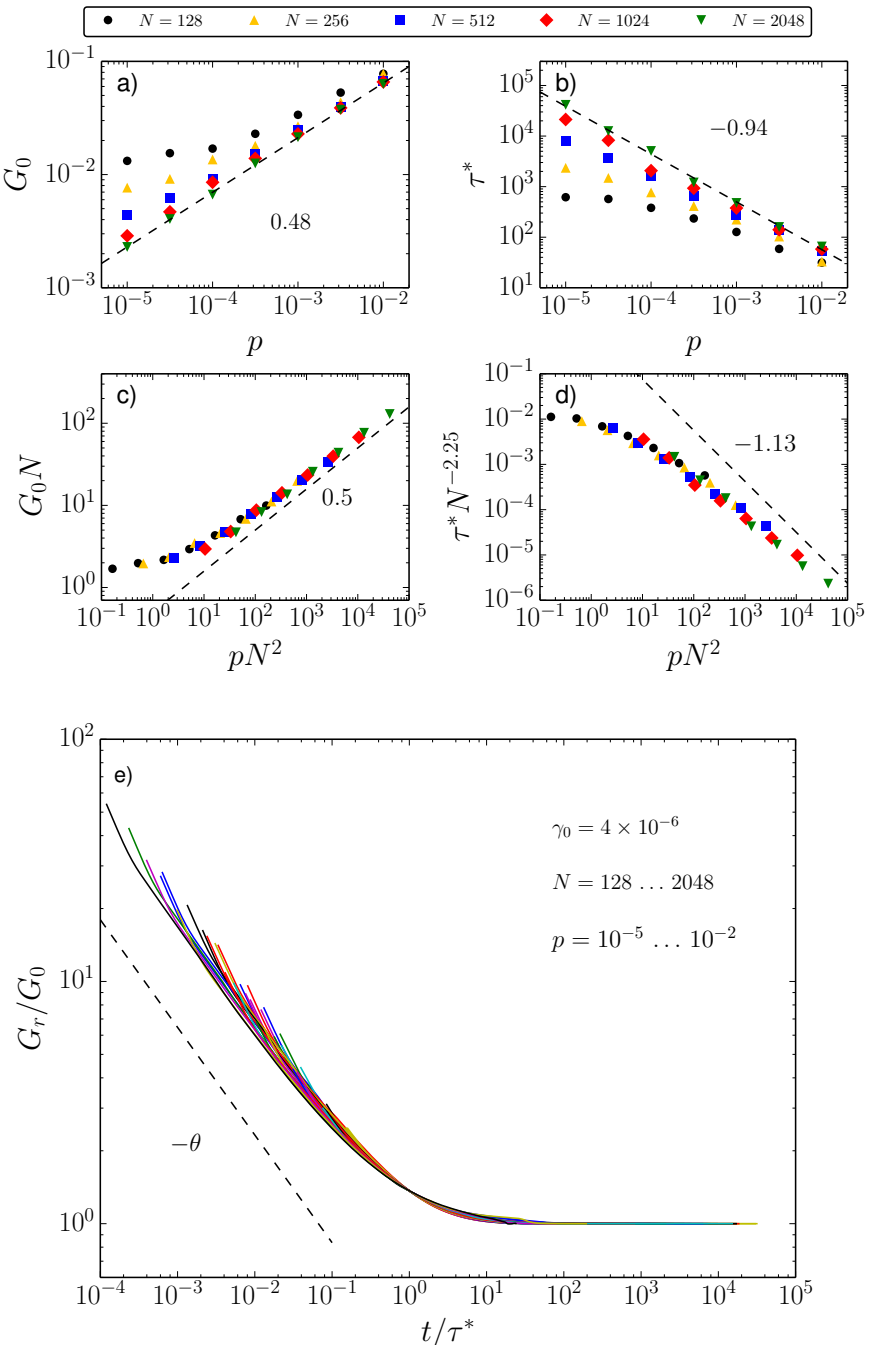

Figure 2.3: (a) The linear shear modulus G_0 in harmonic packings for varying pressure p and number of particles N. (b) The relaxation time τ^* for the same range of p and N as in (a). (c) Finite size scaling collapse of G_0. (d) Finite size scaling collapse of τ^*. (e) The relaxation modulus G_r collapses to a master curve when G_r and t are rescaled with G_0 and τ^*, respectively, as determined in (a) and (b). At short times the master curve decays as a power law with exponent $\theta = \mu/\lambda \approx 0.44$ (dashed line), using the estimates from (c) and (d).

important when a packing has $O(1)$ contacts in excess of isostaticity, or equivalently when $p/k \sim 1/N^2$ – c.f. Eq. (2.6). Consistent with their results, Fig. 2.3a shows clear finite size effects in G_0. Data for different system sizes can be collapsed to a master curve by plotting $G \equiv G_0 N$ versus the rescaled pressure $x \equiv pN^2$. The master curve approaches a power law x^μ consistent with $\mu = 0.5$, as shown in Fig. 2.3c. The scaling of Eq. (2.7), and specifically the value $\mu = 1/2$, is verified by this data collapse, together with the requirement for the modulus to be an intensive property of large systems. To see this, note that G_0 is intensive only if $G \sim x^{1/2}$ for large x.

Again referring to Fig. 2.2, there is clearly some time scale τ^* such that for $t < \tau^*$ the relaxation modulus deviates significantly from the quasistatic modulus. The relaxation time is determined from the point where G_r, averaged over an ensemble of at least 100 packings per condition, has decayed to within a fraction Δ of its final value, $G_r(t = \tau^*) = (1+\Delta)G_0$. We present data for $\Delta = 1/e$, but similar scaling results for a range of Δ.[56] Raw data for varying p and N is shown in Fig. 2.3b. Fitting a power law to the data for $N = 2048$ gives an exponent $\lambda = 0.94$. We now again seek to refine our estimate by collapsing data to a master curve. As τ^* and G_0 are both properties of the relaxation modulus, we require the rescaled pressure to remain $x = pN^2$, which collapses the G_0 data. We then search for data collapse in τ^* by rescaling the relaxation time as $\tau^*/N^{2\lambda}$, which implies that τ^* diverges in large systems in accord with Eq. (2.11). While we find reasonable data collapse for $\lambda = 0.94$, the best collapse occurs for a larger value $\lambda \approx 1.13$, shown in Fig. 2.3d. The theoretical prediction $\lambda = 1$ clearly falls within the range of our numerical estimates,[35] although on the basis of the present data we cannot exclude a slightly different value of λ.

We now use the linear quasistatic modulus G_0 and the characteristic time scale τ^* to collapse the relaxation modulus to a master curve $R(s)$. Fig. 2.3c plots $R \equiv G_r/G_0$ versus $s \equiv t/\tau^*$ for a range of pressures and system sizes; data from the trivial affine regime at times $t < 10\tau_0$ have been excluded. The resulting data collapse is excellent, and the master curve it reveals has two scaling regimes: $R \simeq 1$ for $s \gg 1$, and $R \sim s^{-\theta}$ for $s \ll 1$. The plateau at large s corresponds to the quasistatic scaling $G_r \simeq G_0$. The power law relaxation at shorter times corresponds to $G_r \sim G_0(t/\tau^*)^{-\theta}$ for some exponent θ. By considering a marginal solid prepared at the jamming point, one finds that the prefactor of $t^{-\theta}$ cannot depend on the pressure. Invoking the pressure scaling of G_0 and τ^* in the large N limit, identified above, we conclude that $\theta = \mu/\lambda$. Hence in large systems the relaxation modulus scales as

$$\frac{G_r(t)}{k} \sim \begin{cases} (\tau_0/t)^\theta & 1 \ll t/\tau_0 \ll (k/p)^\lambda \\ (p/k)^\mu & (k/p)^\lambda \ll t/\tau_0 \,. \end{cases} \tag{2.12}$$

with $\mu = 1/2$, $\lambda \approx 1$, and $\theta = \mu/\lambda \approx 0.5$. These findings are consistent with the theoretical predictions in Ref. [35].

Anomalous stress relaxation with exponent $\theta \approx 0.5$ was first observed in simulations below jamming [27] and is also found in disordered spring networks.[70, 71] It is related via Fourier transform to the anomalous scaling of the frequency dependent complex shear modulus $G^* \sim (\imath\omega)^{1-\theta}$ found in viscoelastic solids near jamming.[35] We revisit the scaling relation of Eq. (2.12) in Section 2.4.6.

2.4. Finite strain

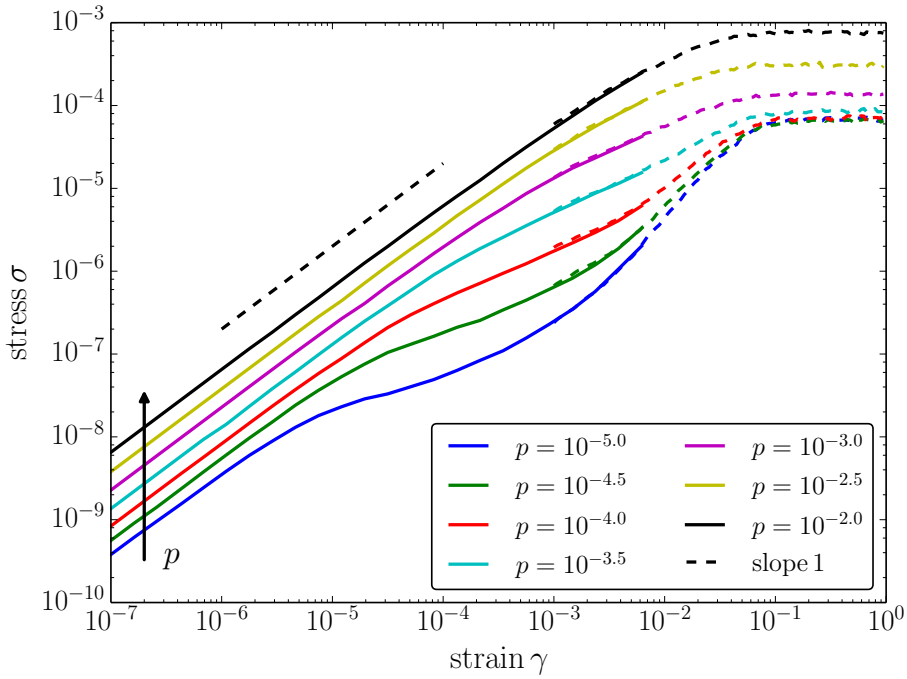

Figure 2.4: Averaged stress-strain curves under quasistatic shear at varying pressure p. Solid and dashed curves were calculated using different strain protocols. Dashed curves: fixed strain steps of 10^{-3}, sheared to a final strain of unity. Solid curves: logarithmically increasing strain steps, beginning at 10^{-9} and reaching a total strain of 10^{-2} after 600 steps.

When does linear elasticity break down under increasing strain, and what lies beyond? To answer these questions, we now probe shear response at finite strain using flow start-up tests.

2.4.1. Flow start-up

In a flow start-up test, strain-controlled boundary conditions are used to "turn on" a flow with constant strain rate $\dot{\gamma}_0$ at time $t = 0$, i.e.

$$\gamma(t) = \begin{cases} 0 & t < 0 \\ \dot{\gamma}_0 t & t \geq 0 \end{cases} \tag{2.13}$$

To implement flow start-up in MD, at time $t = 0$ a packing's particles and simulation cell are instantaneously assigned an affine velocity profile $\vec{v}_i = (\dot{\gamma}_0 \, y_i, 0)^T$ in accordance with a simple shear with strain rate $\dot{\gamma}_0$; the Lees-Edwards images of the simulation cell are assigned a commensurate velocity. Then the particles are allowed to evolve according to Newton's laws while the Lees-Edwards boundary conditions maintain constant velocity, so that the total strain $\gamma(t)$ grows linearly in time.

We also perform quasistatic shear simulations using nonlinear CG minimization to realize the limit of vanishing strain rate. Particle positions are evolved by giving the Lees-Edwards boundary conditions a series of small strain increments and equilibrating to a new minimum of the elastic potential energy. The stress σ is then reported as a function of the accumulated strain. For some runs we use a variable step size in order to more accurately determine the response at small strain.

Fig. 2.1 illustrates the output of both the finite strain rate and quasistatic protocols.

2.4.2. Quasistatic stress-strain curves

To avoid complications due to rate-dependence, we consider the limit of vanishing strain rate first.

Fig. 2.4 plots the ensemble-averaged stress-strain curve $\sigma(\gamma)$ for harmonic packings at varying pressure. Packings contain $N = 1024$ particles, and each data point is averaged over at least 600 configurations. Several features of the stress-strain curves stand out. First, there is indeed a window of initially linear growth. Second, beyond a strain of approximately 5 - 10% the system achieves steady plastic flow and the stress-strain curve is flat. Finally, the end of linear elasticity and the beginning of steady plastic flow do not generally coincide; instead there is an interval in which the stress-strain curve has a complex nonlinear form. We shall refer to the end of the linear elastic regime as "softening" because the stress initially dips *below* the extrapolation of Hooke's law. (In the plasticity literature the same phenomenon would be denoted "strain hardening".) Moreover, for sufficiently low pressures there is a strain interval over which the stress increases faster than linearly. This surprising behavior is worthy of further attention, but the focus of the present work will be on the end of linear elasticity and the onset of softening. This occurs on a strain scale $\gamma^\dagger$ that clearly depends on pressure.

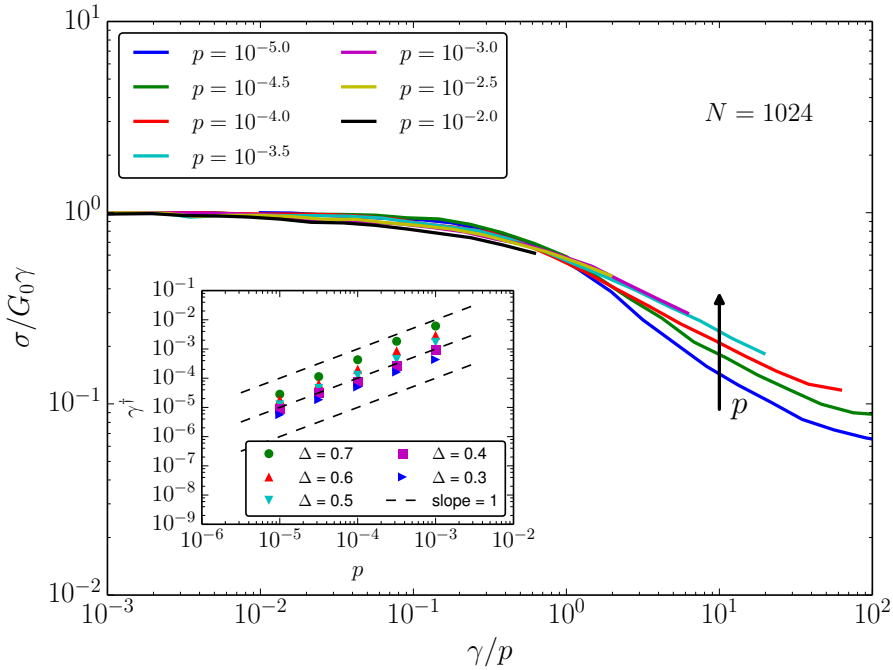

Figure 2.5: (main panel) Data from Fig. 2.4, expressed as a dimensionless effective shear modulus $\sigma/G_0\gamma$ and plotted versus the rescaled strain γ/p. (inset) The crossover strain $\gamma^\dagger$ where the effective shear modulus has decayed by an amount Δ in a system of $N = 1024$ particles.

2.4.3. Onset of softening

We now determine the pressure and system size dependence of the softening (or nonlinear) strain scale $\gamma^\dagger$.

Fig. 2.5 replots the quasistatic shear data from Fig. 2.4 (solid curves), now with the linear elastic trend $G_0\gamma$ scaled out. The rescaling collapses data for varying pressures in the linear regime and renders the linear regime flat. The strain axis in Fig. 2.5b is also rescaled with the pressure, a choice that will be justified below. The onset of softening occurs near unity in the rescaled strain coordinate for all pressures, which suggests that $\gamma^\dagger$ scales linearly with p in harmonic packings ($\alpha = 2$).

Unlike the linear relaxation modulus in Fig. 2.3c, the quasistatic shear data in Fig. 2.5 do not collapse to a master curve; instead the slope immediately after softening steepens (in a log-log plot) as the pressure decreases. As a result, it is not possible to unambiguously identify a correlation $\gamma^\dagger \sim p^\nu$ between the crossover strain and the pressure. To clarify this point, the inset of Fig. 2.5 plots the strain where $\sigma/G_0\gamma$ has decayed by an amount Δ from its plateau value, denoted $\gamma^\dagger(\Delta)$. This strain scale

is indeed approximately linear in the pressure p (dashed curves), but a power law fit gives an exponent ν in the range 0.87 to 1.06, depending on the value of Δ. Bearing the above subtlety in mind, we nevertheless conclude that an effective power law with $\nu = 1$ provides a reasonable description of the softening strain. Section 2.3.1 presents further evidence to support this conclusion.

2.4.4. Hertzian packings

In the previous section the pressure-dependence of $\gamma^\dagger$ was determined for harmonic packings. We now generalize this result to other pair potentials, with numerical verification for the case of Hertzian packings ($\alpha = 5/2$).

Recall that the natural units of stress are set by the contact stiffness k, which itself varies with pressure when $\alpha \neq 2$. Based on the linear scaling of $\gamma^\dagger$ in harmonic packings, we anticipate

$$\gamma^\dagger \sim \frac{p}{k} \sim p^{1/(\alpha-1)}\,, \tag{2.14}$$

which becomes $\gamma^\dagger \sim p^{2/3}$ in the Hertzian case. To test this relation, we repeat the analysis of the preceding Section; results are shown in Fig. 2.6. We again find a finite linear elastic window that gives way to softening. Softening onset can again be described with a Δ-dependent exponent (see inset). Its value has a narrow spread about $2/3$; power law fits give slopes between 0.63 and 0.74.

2.4.5. Relating softening and contact changes

Why does the linear elastic window close when it does? We now seek to relate softening with contact changes on the particle scale.[41–44, 47, 52] Specifically, we identify a correlation between the softening strain $\gamma^\dagger$, the cumulative number of contact changes, and the distance to the isostatic contact number z_c. In so doing we will answer the question first posed by Schreck and co-workers [47], who asked how many contact changes a packing can accumulate while still displaying linear elastic response.

We begin by investigating the ensemble-averaged contact change density $n_{\rm cc}(\gamma) \equiv [N_{\rm make}(\gamma) + N_{\rm break}(\gamma)]/N$, where $N_{\rm make}$ and $N_{\rm break}$ are the number of made and broken contacts, respectively, accumulated during a strain γ. Contact changes are identified by comparing the contact network at strain γ to the network at zero strain.

In Fig. 2.7a we plot $n_{\rm cc}$ for packings of harmonic particles at pressure $p = 10^{-4}$ and varying system size. The data collapse to a single curve, indicating that $n_{\rm cc}$ is indeed an intensive quantity. The effect of varying pressure is shown in Fig. 2.7b. There are two qualitatively distinct regimes in $n_{\rm cc}$, with a crossover governed by pressure.

To better understand these features, we seek to collapse the $n_{\rm cc}$ data to a master curve. By plotting $N \equiv n_{\rm cc}/p^\tau$ versus $y \equiv \gamma/p$, we obtain excellent collapse for $\tau = 1/2$, as shown in Fig. 2.7b for the same pressures as in

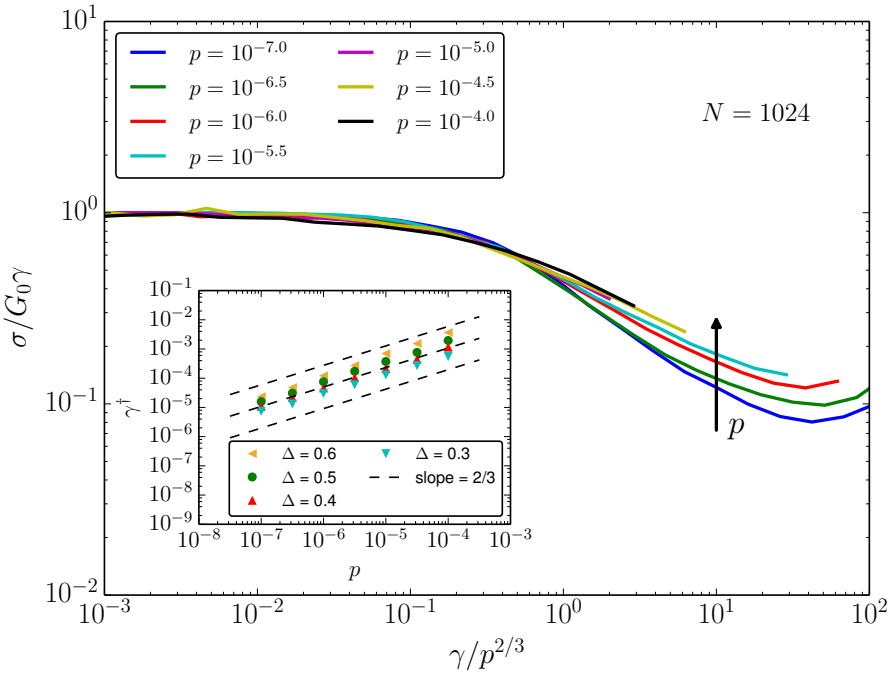

Figure 2.6: (main panel) The dimensionless shear modulus of quasistatically sheared Hertzian packings plotted versus the rescaled strain $\gamma/p^{2/3}$. (inset) Pressure-dependence of the crossover strain $\gamma^\dagger$.

Fig. 2.7a and system sizes $N = 128 \ldots 1024$. The scaling function $N \sim y$ for small y, while $N \sim y^\tau$ for $y \gtrsim 1$. The rescaled strain y provides further evidence for a crossover scale $\gamma^\dagger \sim p/k$, now apparent at the microscale. Moreover, the fact that data for varying system sizes all collapse to the same master curve is an important indicator that $\gamma^\dagger$ is an intensive strain scale that remains finite in the large system size limit.

The scaling collapse in Fig. 2.7c generalizes the results of Van Deen et al. [52], who determined the strain scale $\gamma_{cc}^{(1)} \sim (p/k)^{1/2}/N$ associated with the first contact change. To see this, note that the inverse slope $(\mathrm{d}\gamma/\mathrm{d}n_{cc})/N$ represents the average strain interval between contact changes at a given strain. Hence the initial slope of n_{cc} is fixed by $\gamma_{cc}^{(1)}$,

$$n_{cc}(\gamma) \simeq \frac{1}{N}\left(\frac{\gamma}{\gamma_{cc}^{(1)}}\right) \tag{2.15}$$

as $\gamma \to 0$. From Fig. 2.7 it is apparent that n_{cc} remains linear in γ up to the crossover strain $\gamma^\dagger$. We conclude that $\gamma_{cc}^{(1)}$ describes the strain between successive contact changes over the entire interval $0 < \gamma < \gamma^\dagger$. In the

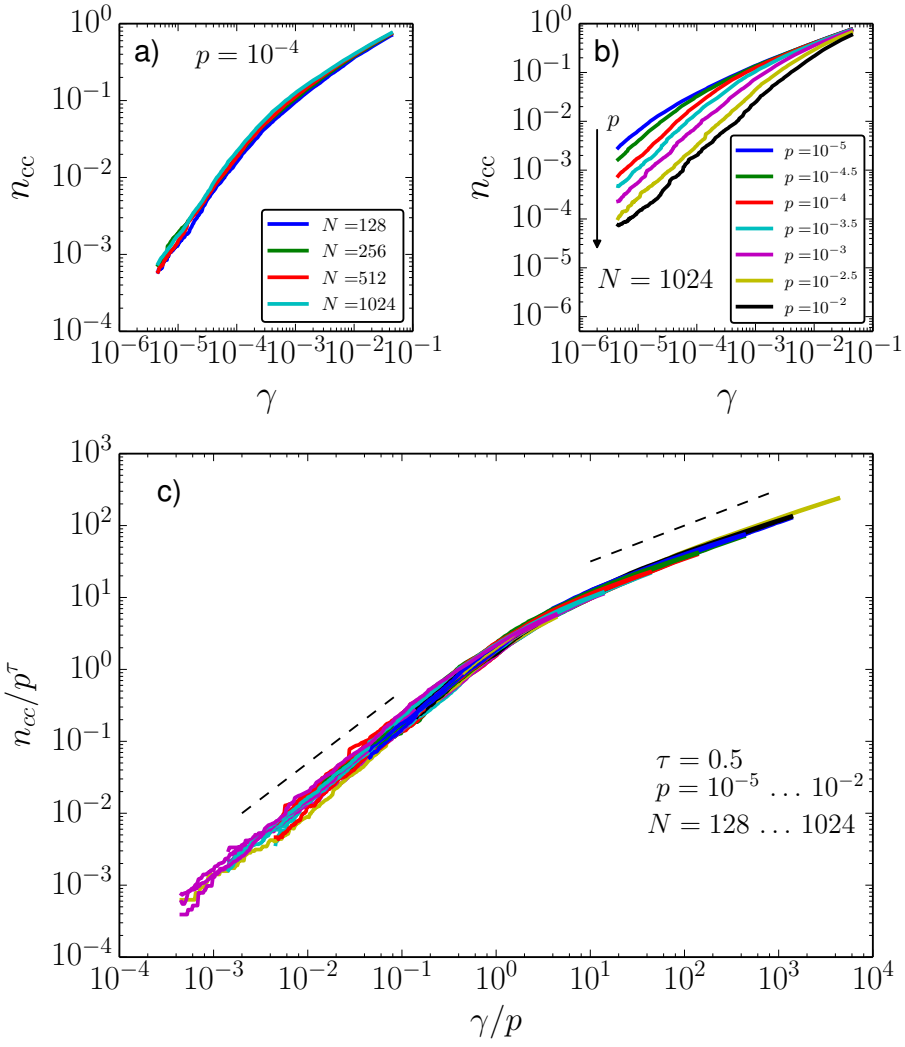

Figure 2.7: The contact change density shown for (a) varying system size and (b) varying pressure. (c) Data collapse for pressures $p = 10^{-2} \ldots 10^{-5}$ in half decade steps and system sizes $N = 128 \ldots 1024$ in multiples of 2. Dashed lines indicate slopes of 1 and 1/2.

softening regime the strain between contact changes increases; it scales as $n_{cc} \sim \gamma^{1/2}$ (see Fig. 2.7c). This corresponds to an increasing and strain-dependent mean interval $\gamma^{1/2}/N$ between contact changes.

Let us now re-interpret the softening crossover strain $\gamma^{\dagger} \sim \Delta z^2$ (c.f. Eq. (2.6)) in terms of the coordination of the contact network. We recall that $\Delta z = z - z_c$ is the difference between the initial contact number z and the

isostatic value z_c, which corresponds to the minimum number of contacts per particle needed for rigidity. The excess coordination Δz is therefore an important characterization of the contact network. The contact change density at the softening crossover, $n_{\rm cc}^{\dagger}$, can be related to Δz via Eq. (2.15), while making use of Eq. (2.6),

$$n_{\rm cc}^{\dagger} \equiv n_{\rm cc}(\gamma^{\dagger}) \sim \Delta z\,. \tag{2.16}$$

Hence we have empirically identified a topological criterion for the onset of softening: an initially isotropic packing softens when it has undergone an extensive number of contact changes that is comparable to the number of contacts it initially had in excess of isostaticity. Note that this does not mean the packing is isostatic at the softening crossover, as $n_{\rm cc}$ counts both made and broken contacts.

2.4.6. Rate-dependence

To this point we have considered nonlinear response exclusively in the limit of quasistatic shearing. A material accumulates strain quasistatically when the imposed strain rate is slower than the longest relaxation time in the system. Because relaxation times near jamming are long and deformations in the lab always occur at finite rate, we can anticipate that quasistatic response is difficult to achieve and that rate-dependence generically plays a significant role. Hence it is important to consider shear at finite strain and finite strain rate. We now consider flow start-up tests in which a finite strain rate $\dot{\gamma}_0$ is imposed at time $t = 0$, cf. Eq. (2.13).

Fig. 2.8 displays the mechanical response to flow start-up for varying strain rates. To facilitate comparison with the quasistatic results of the previous section, data are plotted in terms of the dimensionless quantity $\sigma(t;\dot{\gamma}_0)/G_0\gamma$, which we shall refer to as the effective shear modulus. The data are for systems of $N = 1024$ particles, averaged over an ensemble of around 100 realizations each. Here we plot data for the pressure $p = 10^{-4}$; results are qualitatively similar for other pressures. For comparison, we also plot the result of quasistatic shear (solid circles) applied to the same ensemble of packings.

Packings sheared sufficiently slowly follow the quasistatic curve; see e.g. data for $\dot{\gamma}_0 = 10^{-11}$. For smaller strains, however, the effective shear modulus is stiffer than the quasistatic curve and decays as $\sigma/\gamma \sim t^{-\theta}$ (see inset). This is rate-dependence: for a given strain amplitude, the modulus increases with increasing strain rate. Correspondingly, the characteristic strain γ^* where curves in the main panel of Fig. 2.8 reach the linear elastic plateau ($\sigma/G_0\gamma \approx 1$) grows with $\dot{\gamma}_0$. For sufficiently high strain rates there is no linear elastic plateau; for the data in Fig. 2.8 this occurs for $\dot{\gamma}_0 \approx 10^{-8}$. Hence there is a characteristic strain rate, $\dot{\gamma}^{\dagger}$, beyond which the linear elastic window has closed: packings sheared faster than $\dot{\gamma}^{\dagger}$ are always rate-dependent and/or strain softening.

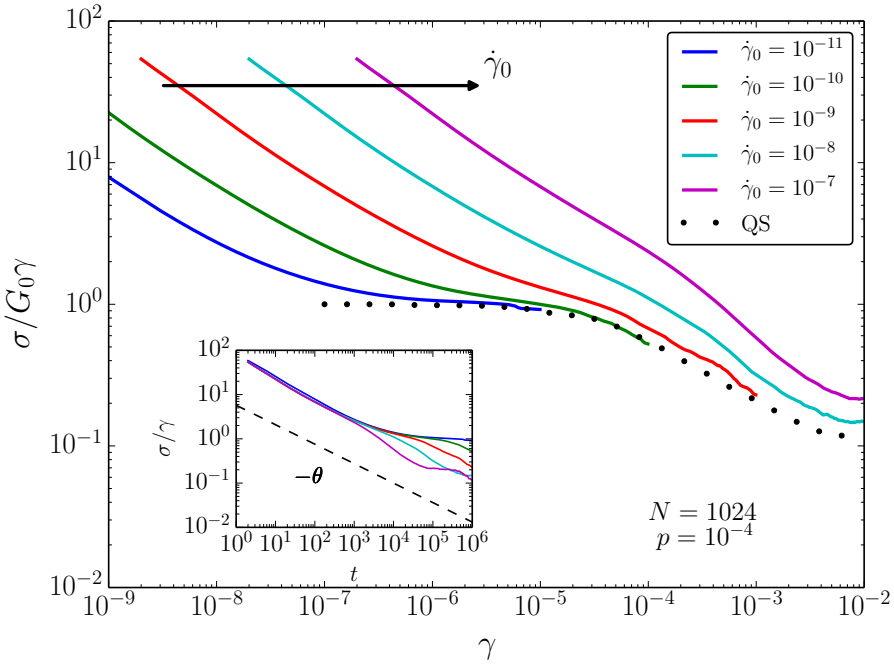

Figure 2.8: The effective shear modulus during flow start-up for packings of $N = 1024$ particles at pressure $p = 10^{-4}$, plotted versus strain for varying strain rates $\dot{\gamma}_0$. (inset) The same data collapses for early times when plotted versus t, decaying as a power law with exponent $\theta = \mu/\lambda \approx 0.44$ (dashed line).

To understand the rate-dependent response at small strains, we revisit the relaxation modulus determined in Section 2.3. In linear response the stress after flow start-up depends only on the elapsed time $t = \gamma/\dot{\gamma}_0$,

$$\frac{\sigma}{\gamma} = \frac{1}{t}\int_0^t G_r(t')\,\mathrm{d}t' \,. \tag{2.17}$$

Employing the scaling relations of Eq. (2.12), one finds

$$\frac{\sigma}{\gamma} \sim k\left(\frac{\tau_0}{t}\right)^{\theta}, \qquad \tau_0 < t < \tau^* \,, \tag{2.18}$$

as verified in Fig. 2.8 (inset). Linear elasticity $\sigma/\gamma \simeq G_0$ is only established at longer times, when $\gamma > \dot{\gamma}_0\tau^* \sim (k/p)^{\lambda}\,\dot{\gamma}_0\tau_0$. Hence the relaxation time τ^* plays an important role: it governs the crossover from rate-dependent to quasistatic linear response. The system requires a time τ^* to relax after a perturbation. When it is driven at a faster rate, it cannot relax fully and hence its response depends on the driving rate.

We can now identify the characteristic strain rate $\dot{\gamma}^\dagger$ where the linear elastic window closes. This rate is reached when the bound on quasistaticity, $\gamma > \dot{\gamma}_0 \tau^*$, collides with the bound on linearity, $\gamma < \gamma^\dagger$, giving

$$\dot{\gamma}^\dagger \sim \frac{(p/k)^{1+\lambda}}{\tau_0}\,, \tag{2.19}$$

with $1 + \lambda \approx 2$. This strain rate vanishes rapidly near jamming, hence packings must be sheared increasingly slowly to observe a stress-strain curve that obeys Hooke's law.

2.5. Implications for experiment

The time scale τ^*, strain scales γ^* and $\gamma^\dagger$, and strain rate $\dot{\gamma}^\dagger$ all place bounds on the window of linear elastic response. Which of these quantities are most relevant depends on the particular rheological test one performs. For example, in a flow start-up test Hooke's Law is accurate within the window $\gamma^* < \gamma < \gamma^\dagger$, provided the strain rate $\dot{\gamma}_0 < \dot{\gamma}^\dagger$. This is the scenario depicted in Fig. 2.1; it is also illustrated schematically in Fig. 2.9. In a stress relaxation test, however, the strain amplitude and test duration can be varied independently. Hooke's law is then accurate for $\gamma_0 < \gamma^\dagger$ provided one waits for a time $t > \tau^*$ for the system to relax. (We have verified that the softening onset still occurs at $\gamma^\dagger$ when the full strain γ_0 is applied in one step, as opposed to a quasistatic series of small steps.) Similar parameter ranges can be constructed for other rheological tests.

What experimental scales do these quantities correspond to? Most importantly, one must collect data in the scaling regime near jamming. Quantities such as the excess coordination and moduli show gradual deviations from scaling when the excess volume fraction exceeds $\Delta\phi \approx 10^{-1}$.[72] Determining the volume fraction with an accuracy better than 1% is difficult[59, 73, 74], hence the experimentally accessible scaling regime is typically just one decade wide in $\Delta\phi$.

The onset of softening occurs at a strain scale $\gamma^\dagger \sim (p/k) \sim \Delta\phi$. If we take the smallest experimentally accessible value of $\Delta\phi$ to be 10^{-2}, then Hooke's law can (potentially) be observed for strains on the order of 1% and smaller.

To estimate the scales τ^*, γ^*, and $\dot{\gamma}^\dagger$, one must know the microscopic time scale τ_0, which arises from a balance between viscous and elastic forces. Simple dimensional analysis then suggests a time scale on the order of $\eta d/\gamma_s$, where η is the viscosity of the continuous phase, d is a typical bubble size, and γ_s is the surface tension.[75] In dishwasher detergent, for example, viscosities are on the order of 1 mPa·s and surface tensions $\gamma_s \sim 10$ mN/m, while bubble sizes can from 100 μm to 1 cm.[76, 77] Hence microscopic time scales fall somewhere in the range $10^{-5} \ldots 10^{-3}$ s. For $\Delta\phi$ on the order 10^{-2}, the time scale $\tau^* \sim \tau_0/(p/k) \sim \tau_0/\Delta\phi$ remains shorter

than 0.1 s at accessible values of $\Delta\phi$, while $\dot{\gamma}^{\dagger} \sim \Delta\phi^2/\tau_0$ can be as low as 0.1 s^{-1}.

We offer a note of caution when considering bounds involving the time scale τ_0. First, experiments find power law relaxation at volume fractions deep in the jammed phase.[78] There is an associated time scale that can be on the order of 1 s depending on sample age, which is significantly longer than our estimates of τ_0 above. This suggests that coarsening and details of the continuous phase flow within thin films and Plateau borders may play an important role – in addition to the strongly non-affine motion associated with proximity to jamming [35, 79] – yet neither are incorporated in Durian's bubble model.[7] Second, while we have considered dissipation proportional to the relative velocity of contacting particles, the viscous force law need not be linear. In foams, for example, the dominant source of damping depends sensitively on microscopic details such as the size of the bubbles and the type of surfactant used.[76] Often one finds Bretherton-type damping proportional to (relative) velocity to the power 2/3.[77, 80] We anticipate that nonlinear damping would impact the relaxation dynamics [25, 81, 82] and alter the value of the exponents θ and λ. For sufficiently long times or slow shearing above ϕ_c, however, we expect particles to follow quasistatic trajectories and the differences between various methods of damping to become negligible.

2.6. Discussion

Using a combination of stress relaxation and flow start-up tests, we have shown that soft solids near jamming are easily driven out of the linear elastic regime. There is, however, a narrow linear elastic window that survives the accumulation of an extensive number of contact changes. This window is bounded from below by viscous dissipation and bounded from above by the onset of strain softening due to plastic dissipation. Close to the transition these two bounds collide and the linear elastic window closes. Hence marginal solids are easily driven into rate-dependent and/or strain softening regimes on at volume fractions and strain scales relevant to the laboratory. Fig. 2.9 provides a qualitative summary of our results for the case of flow start-up.

While our simulations are in two dimensions, we expect the scaling relations we have identified to hold for $D > 2$. To the best of our knowledge, all scaling exponents near jamming that have been measured in both 2D and 3D are the same. There is also numerical evidence that $D = 2$ is the transition's upper critical dimension.[54, 69]

Our work provides a bridge between linear elasticity near jamming, viscoelasticity at finite strain rate, and nonlinearity at finite strain amplitude. The measured relaxation modulus G_r is in good agreement with the linear viscoelasticity predicted by Tighe,[35] as well as simulations by Hatano conducted in the unjammed phase.[27] Our findings regarding the crossover to nonlinear strain softening can be compared to several

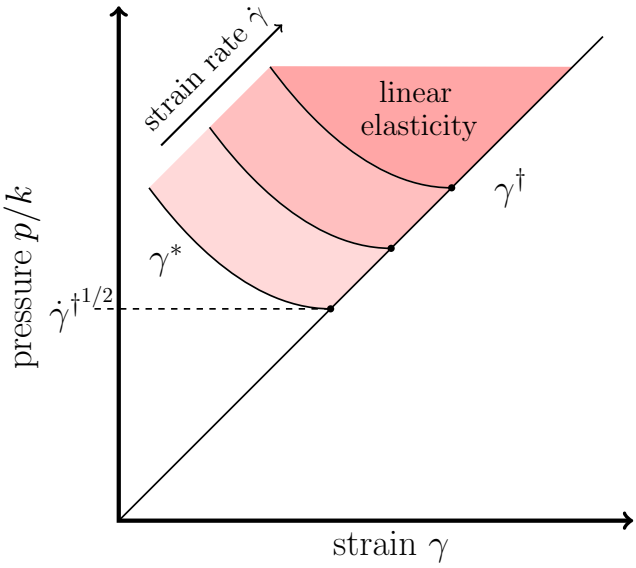

Figure 2.9: In a flow start-up test, quasistatic linear response ($G \approx G_0$) occupies a strain window $\gamma^* < \gamma < \gamma^\dagger$ (shaded regions). For smaller strains the response is rate-dependent, with a crossover strain γ^* that depends on both pressure and strain rate. Softening sets in for higher strains, with a crossover $\gamma^\dagger$ that depends only on the pressure. The intersection of the rate-dependent and softening crossovers defines a strain rate $\dot{\gamma}^\dagger$ above which there is no quasistatic linear response, i.e. the shaded region closes.

prior studies. The granular experiments of Coulais et al. show softening, although their crossover strain scales differently with the distance to jamming, possibly due to the presence of static friction.[33] The emulsions of Knowlton et al. are more similar to our simulated systems, and do indeed display a crossover strain that is roughly linear in $\Delta\phi$, consistent with our $\gamma^\dagger$.[41] A recent scaling theory by Goodrich et al.[57], by contrast, predicts a crossover strain $\gamma^\dagger \sim \Delta\phi^{3/4}$, which is excluded by our data. Nakayama et al.[55] claim agreement between their numerical data and the theoretical exponent $3/4$, although they note that their data is also compatible with a linear scaling in $\Delta\phi$. A recent study by Otsuki and Hayakawa [34] also finds a strain scale proportional to $\Delta\phi$ in simulations of large amplitude oscillatory shear at finite frequency. The agreement between the crossover strains in our quasistatic simulations and these oscillatory shear simulations is surprising, as most of the latter results are for frequencies higher than $\dot{\gamma}^\dagger$, where viscous stresses dominate. There are also qualitative differences between the quasistatic shear modulus, which cannot be collapsed to a master curve (Fig. 2.5), and the storage modulus in oscillatory shear, which can.[34, 56] We speculate that there are corresponding microstructural differences between packings in steady state and transient shear, [40] similar to those which produce memory effects.[83]

Soft sphere packings near jamming approach the isostatic state, which also governs the rigidity of closely related materials such as biopolymer and fiber networks.[84–87] It is therefore remarkable to note that, whereas sphere packings soften under strain, quasistatically sheared amorphous networks are strain stiffening beyond a crossover strain that scales as Δz [88], which vanishes more slowly than $\gamma^\dagger \sim \Delta z^2$ in packings. Hence nonlinearity sets in later and with opposite effect in networks.[89] We expect that this difference is attributable to contact changes, which are absent or controlled by slow binding/unbinding processes in networks.

We have demonstrated that softening occurs when the system has accumulated a finite number of contact changes correlated with the system's initial distance from the isostatic state. This establishes an important link between microscopic and bulk response. Yet further work investigating the relationship between microscopic irreversibility, softening, and yielding is needed. The inter-cycle diffusivity in oscillatory shear, for example, jumps at yielding [41, 44], but its pressure dependence has not been studied. Shear reversal tests could also provide insight into the connection between jamming and plasticity.

While the onset of softening can be probed with quasistatic simulation methods, rate dependent effects such as the strain scale γ^* should be sensitive to the manner in which energy is dissipated. The dissipative contact forces considered here are most appropriate as a model for foams and emulsions. Hence useful extensions to the present work might consider systems with, e.g., lubrication forces or a thermostat.

3

Stress Relaxation

We report the results of molecular dynamics simulations of stress relaxation tests in athermal viscous soft sphere packings close to their unjamming transition. By systematically and simultaneously varying both the amplitude of the applied strain step and the pressure of the initial condition, we access both linear and nonlinear response regimes and control the distance to jamming. Stress relaxation in viscoelastic solids is characterized by a relaxation time τ^* that separates short time scales, where viscous loss is substantial, from long time scales, where elastic storage dominates and the response is essentially quasistatic. We identify two distinct plateaus in the strain dependence of the relaxation time, one each in the linear and nonlinear regimes. The height of both plateaus scales as an inverse power law with the distance to jamming. By probing the time evolution of particle velocities during relaxation, we further identify a correlation between mechanical relaxation in the bulk and the degree of non-affinity in the particle velocities on the micro scale.

This chapter is based on the following publication: J. Boschan, S.A. Vasudevan, P.E. Boukany, E. Somfai, B.P. Tighe, Stress relaxation in viscous soft spheres, Soft Matter, 13, 6870-6876, (2017).

3.1. Introduction

Viscoelasticity is associated with one or more time scales that reflect the changing balance between viscous loss and elastic storage as a material's response to mechanical perturbations evolves in time.[23, 90] Here we implement a standard rheometric test of viscoelasticity, namely stress relaxation in response to an instantaneous step strain, and apply it to a minimal numerical model for foams, emulsions, and soft colloidal suspensions. [7]

Our focus is on athermal systems close to the nonequilibrium (un)jamming transition, where the material develops rigidity under compression. [4, 24, 30] Because the shear modulus vanishes continuously at the jamming point, weakly jammed states near the transition can be arbitrarily soft.[4] Intuition then suggests that their linear response window should also be narrow – small changes in strain amplitude should suffice to drive weakly jammed materials from linear to nonlinear response. Numerics confirm this expectation; under quasistatic shear, for example, the strain scales where the first contact change occurs and where bulk softening sets in both vanish as power laws with the pressure.[52, 91, 92] While there has recently been considerable interest in nonlinear response near jamming,[33, 34, 36, 45–47, 52, 88, 89, 91–96] the form of the relaxation time for large strain steps remains an important open question. Here we demonstrate for the first time that, as the system passes from linear to nonlinear response, relaxation times depend not only on the material constitution, but also on the amplitude of a shear perturbation.

A diverging relaxation time is an important mechanical property of soft amorphous matter near jamming.[3, 35, 97] In the jammed phase, the stress relaxation time τ^* describes the time needed to reach a new mechanical equilibrium after a sudden shear strain.[92] In linear response, the divergence of τ^* as the confining pressure p is sent to zero signals the loss of rigidity.[35] The unjammed phase displays a similarly growing time scale, which marks a crossover from power law to exponential stress relaxation.[27] Both linear and nonlinear stress relaxation can be characterized with the relaxation modulus $G_r(t, \gamma_0)$, which describes the time evolution of the shear stress $\sigma(t, \gamma_0)$ after a step strain with amplitude γ_0,

$$G_r(t, \gamma_0) = \frac{\sigma(t, \gamma_0)}{\gamma_0} \,. \tag{3.1}$$

For infinitesimal γ_0, the stress is directly proportional to the strain and G_r is a function of time alone. In this limit the relaxation modulus is equivalent (i.e. related by standard mathematical transformations) to other common rheometric tests, including small amplitude oscillatory shear and flow start-up.[23] In the nonlinear regime this equivalence generally breaks down.

Existing theoretical [35] and numerical[92] studies of G_r near jamming are valid only in the linear response regime. Its typical form is illus-

trated in Fig. 3.1. After a brief plateau at short times, G_r undergoes a power law decay before reaching a quasistatic plateau. The relaxation time is the time needed to reach the quasistatic plateau. In linear response it diverges as an inverse power law with p.[35, 70, 92, 98] Numer-

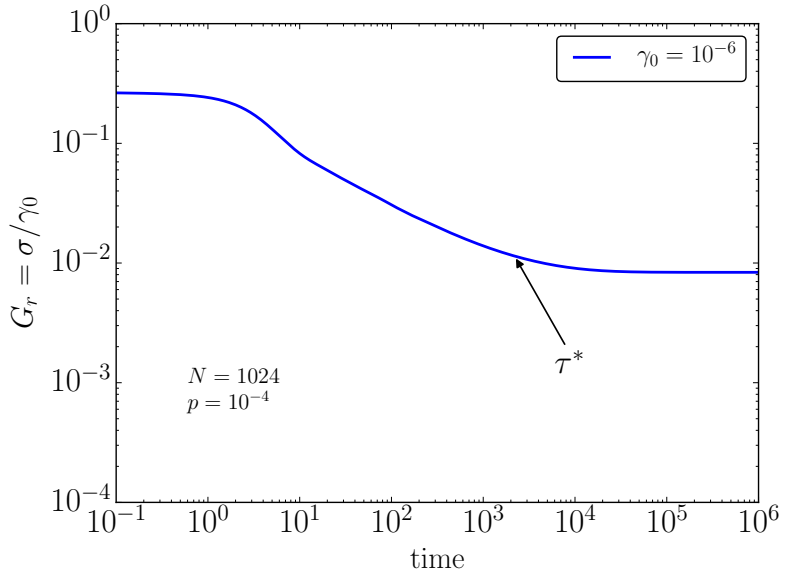

Figure 3.1: The time evolution of the shear relaxation modulus G_r, calculated for a step strain with amplitude $\gamma_0 = 10^{-6}$ at pressure $p = 10^{-4}$ and $N = 1024$. The characteristic relaxation time τ^* is identified as the point where G_r reaches $1 + 1/e$ times its quasistatic plateau value.

ical studies of nonlinear response near jamming typically neglect rate-dependent effects by focusing on quasistatic shear.[34, 52, 91, 92, 94] They have identified two important linear-to-nonlinear crossover strain scales. The first corresponds to the breakdown of linear response on the scale of individual particle trajectories, which is driven by changes to the contact network.[45–47, 52, 91, 92] The contact change strain scales as $\gamma_{cc} \sim p^{1/2}/N$.[52, 91, 92] The second characteristic strain corresponds to softening, i.e. the loss of linearity in the average stress-strain curve. It scales as $\gamma^\dagger \sim p$.[34, 92, 94] Note that these two strains scale differently with p; we will revisit this observation below.

In the present work we study the linear and nonlinear relaxation time of weakly jammed solids over a wide range in pressure and strain amplitude γ_0 connecting linear and nonlinear response. Our central finding is that the relaxation time as a function of γ_0 displays two plateaus: one in the linear regime, and a second, higher plateau at larger strains. The pressure dependence of these two plateaus is identical, i.e. they diverge as power laws with the same exponent. This is a surprising result, as there is no

a priori reason for their exponents to be the same. We further relate the form of τ^* to the time evolution of floppy-like, non-affine particle motions during relaxation.

3.2. Methods and Model

Foams are modeled with the Durian bubble model [7] in two dimensions. Bubbles are represented as disks that repel elastically when they overlap, with an additional dissipative force proportional to their relative velocity. The elastic force between particles i and j is proportional to their overlap $\delta_{ij} = (R_i + R_j) - r_{ij}$, where R_i and R_j denote the radii and r_{ij} is the length of the vector $\vec{r}_{ij}$, pointing from the center of particle i to the center of particle j,

$$\vec{f}_{ij}^{\,\mathrm{el}} = \begin{cases} -k(\delta_{ij})\delta_{ij}\hat{r}_{ij}, & \text{if } \delta_{ij} > 0 \\ \vec{0}, & \text{otherwise.} \end{cases} \tag{3.2}$$

The viscous force depends on the relative velocity v_{ij} of the touching particles evaluated at the contact,

$$\vec{f}_{ij}^{\,\mathrm{v}} = \begin{cases} -\tau_0 k \mathrm{v}_{ij}, & \text{if } \delta_{ij} > 0 \\ \vec{0}, & \text{otherwise,} \end{cases} \tag{3.3}$$

where τ_0 is the microscopic relaxation time. All material properties are expressed in dimensionless units constructed from k, τ_0, and the mean bubble size.

The stress tensor is

$$\sigma_{\alpha\beta} = \frac{1}{2V} \sum_{ij} \mathrm{f}_{ij,\alpha} \mathrm{r}_{ij,\beta} - \frac{1}{V} \sum_{i} m_i \mathrm{v}_{i,\alpha} \mathrm{v}_{i,\beta}, \tag{3.4}$$

where Greek indices denote Cartesian coordinates. The contact stress term contains the total force at each contact, $\mathrm{f}_{ij} = \mathrm{f}_{ij}^{\mathrm{el}} + \mathrm{f}_{ij}^{\mathrm{v}}$. The inertial stress is dictated by the center of mass velocity v_i. Each particle has unit density, so its mass m_i is proportional to its area. V is the total area of the unit cell. The inertial stress term is negligible for times longer than the damping time τ_0.

Initial conditions are created by randomly populating the simulation box and then using an energy minimization protocol to quench instantaneously to a local minimum of the elastic potential energy at fixed volume. The box is then allowed to undergo small changes in size and shape to achieve a target pressure p and zero shear stress – these are called "shear-stabilized" packings in the nomenclature of Dagois-Bohy et al.[60] The pressure provides a convenient measure of proximity to the (un)jamming point at $p = 0$. Packings are bidisperse to avoid crystallization; we use the standard[4, 6] 50-50 mixture of small and large particles and a radius ratio of 1:1.4. Once the initial state is prepared, we use molecular

dynamics simulations to apply shear, which allows us to resolve the time evolution of the system. Newton's laws are integrated using a velocity Verlet algorithm.

3.3. Stress relaxation at finite strain

In order to describe the mechanical relaxation of soft sphere packings, we investigate the system's shear stress in response to an instantaneous step strain of amplitude γ_0 applied at time $t = 0$. The strain is imposed using Lees-Edwards periodic boundary conditions while displacing the particles' coordinates (x_i, y_i) affinely according to $(x_i, y_i) \to (x_i + \gamma_0 y, y_i)$. In order to stay clear of any spurious periodic signatures in our results, we restrict applied strains to $\gamma_0 < 0.01$; this is still large enough to observe the softening crossover for the highest pressure we simulate, as discussed below. For times $t > 0$ after the instantaneous shear, the periodic boundaries are kept fixed in their strained position and the particles are allowed to relax to a new mechanical equilibrium. The resulting stress relaxation is illustrated in Fig. 3.1, which shows the relaxation modulus $G_r(t, \gamma_0)$ as a function of time t for a single strain amplitude and pressure.

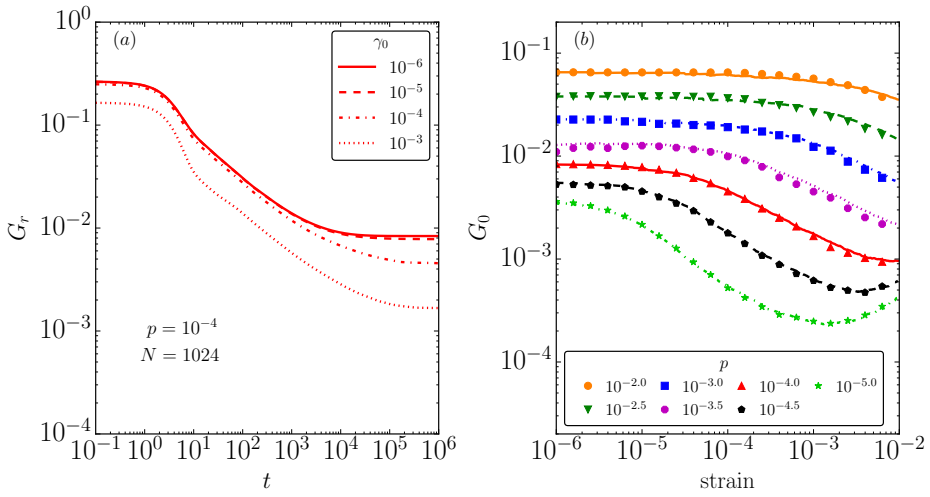

Figure 3.2: (a) The time evolution of the shear relaxation modulus G_r for $p = 10^{-4}$ and $N = 1024$ at different strain amplitudes (see legend). (b) The quasistatic, long time shear modulus G as a function of strain. The data points show the long time response to instantaneous step strains. The lines are results from a separate set of simulations that reach the same total strain via a series of incremental steps applied using a quasistatic shear protocol.

The relaxation modulus displays several noteworthy features. There is an initial plateau at times shorter than the damping time $\tau_0 \equiv 1$, which occurs because viscous forces inhibit the system from relaxing at a rate faster than $1/\tau_0$. On longer time scales, the shear modulus decreases as a

power law $1/t^{\theta}$ with an exponent $\theta = 1/2$.[35, 92] This relaxation continues until the stress reaches a second, long time plateau. The height of the plateau defines a quasistatic modulus $G(\gamma_0)$, which approaches the linear elastic shear modulus $G_0 = G(0)$ in the limit of vanishing strain amplitude. The crossover between power law relaxation and the quasistatic plateau defines the relaxation time $\tau^*(\gamma_0)$.

Fig. 3.2a illustrates the evolution of the relaxation modulus with increasing strain amplitude at a pressure $p = 10^{-4}$, which is representative of the entire range of pressures simulated here. All curves show qualitatively similar time evolution. However, there is a crossover with increasing γ_0. For the small values $\gamma_0 = 10^{-6}$ and 10^{-5} (solid and dashed curves), the relaxation modulus collapses, which is indicative of linear response. For higher strain amplitudes, beginning here around $\gamma_0 = 10^{-4}$, the entire curve shifts downward. This is strain softening. Softening is also evident in the quasistatic modulus $G(\gamma_0)$, estimated from $G_r(t = 10^6, \gamma_0)$, which we plot in Fig. 3.2b for varying pressures (symbols). At low strains the modulus remains constant, consistent with linear response. Softening corresponds to a subsequent decrease in $G(\gamma_0)$ with increasing γ_0. This general trend is evident at all pressures.

Strain softening has been explored previously in Ref. [92], where it was found that the onset of softening occurs at a strain scale proportional to p, after a finite fraction of the particles have undergone contact changes. There shear was built up incrementally using a quasistatic protocol, so that the final amplitude γ_0 was reached via a large number of small steps $\Delta\gamma$. Once linear response has broken down and the system has begun to soften, however, there is no fundamental reason that the result of an incremental quasistatic protocol should correspond to the long time limit of viscoelastic relaxation after a single large step strain. It is therefore surprising that when we overplot the results for incremental strain from Ref. [92] (solid curves), we find near perfect agreement between the two data sets. This suggests that, on average, the two protocols reach the same minimum in the energy landscape of the sheared system.

3.4. Relaxation time and strain dependence

We now investigate the time $\tau^*(\gamma_0)$ needed to reach the quasistatic plateau after a strain of amplitude γ_0. While linear response can be accessed with careful numerical experiments,[35, 92] one would prefer to have a complete characterization of the dependence of the relaxation time, not just on p, but also on the amplitude γ_0 of the strain step. Our main result is the observation of a plateau in τ^* at large γ_0, with pressure dependence comparable to the relaxation time in linear response.

We identify τ^* as the time when the relaxation modulus reaches a value $1 + \Delta$ times its value in the long time plateau. In the following we set $\Delta = 1/e$; we have verified that our results are representative of a range of values for Δ. We simulate relaxation time measurements for stress relax-

ation over three decades in pressure, $p = 10^{-2} ... 10^{-5}$, and four decades in strain amplitude, $\gamma_0 = 10^{-6} ... 10^{-2}$. Results are averaged over at least 500 realizations per condition. In MD simulations the total simulated time is limited by the available computational resources; especially for the lowest pressures and largest strain amplitudes, one can ask if the system might relax yet more at longer times. To exclude this possibility, we have also performed quasistatic simulations using the FIRE algorithm [22] to determine the long time limit of the shear modulus. We then recalculate the relaxation time using the quasistatic plateau value, in combination with the time evolution of the MD simulation. These results are in good agreement with the relaxation times calculated directly from MD. Hence we are confident that our results are representative of fully relaxed packings.

The evolution of the relaxation time, plotted in Fig. 3.3, can be separated into three stages. At low strains, the response is linear and the plot of τ^* *versus* γ_0 plateaus, with the height of the plateau determined by the pressure. Next there is a second, intermediate regime, where linear response breaks down and the relaxation time begins to grow with increasing strain amplitude. The crossover causes the relaxation time to increase by approximately one order of magnitude. Finally, there is a regime at comparably high strains where τ^* develops a second plateau. This trend continues throughout the studied pressure range, with the crossover shifting to higher strains with increasing pressure. As a result, the linear response window is at the edge of the sampled strain range for the lowest pressures, while the nonlinear plateau is only beginning to develop for the highest pressure.

In order to highlight pressure dependence, we seek to collapse the relaxation time data by plotting τ^*/p^λ *versus* γ_0/p^ν. We select $\lambda = 0.85$, which is the relaxation time exponent identified numerically in our prior study of strictly linear response,[92] and close to the theoretically predicted value of 1.[35] For the strain axis rescaling we select $\nu = 0.5$, which is characteristic of the contact change strain scale γ_{cc} discussed above.[52, 91, 92] This choice is motivated by comparing Figs. 3.2b and 3.3, where one observes that the upturn in τ^* for increasing γ_0 always occurs at a strain where the quasistatic shear modulus is still approximately flat, i.e. before the onset of softening. The rescaled data, plotted in Fig. 3.4, show good collapse over the entire range of strains and pressures. There is a small departure for the lowest pressure (i.e. closest to jamming) at the highest strain amplitudes, which may be associated with finite size effects.

The data collapse in Fig. 3.4 indicates one of our central results, namely that the relaxation time plateaus at low and high strains diverge as inverse power laws with p, with the same characteristic exponent λ. We consider this result surprising, as there is no fundamental reason that the divergence of the relaxation times at finite strains should comply with the form for infinitesimal strain. The rescaling of the strain axis with $p^{0.5}$, and the position of the crossover at a value $\gamma_0/p^{0.5} \sim O(1/N)$, strongly suggest

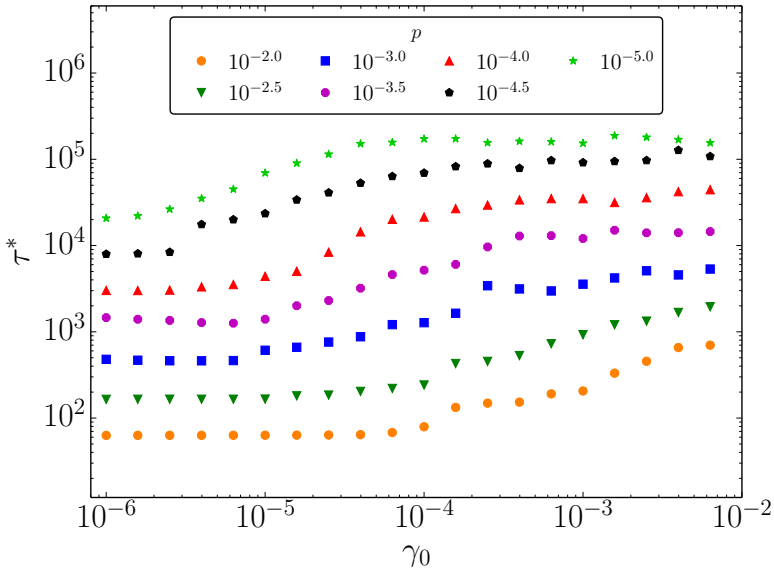

Figure 3.3: The relaxation time τ^* as a function of strain γ_0 for system size $N = 2048$ and varying pressures, $p = 10^{-5} \ldots 10^{-2}$ (see legend).

that the increase in relaxation time is associated with the onset of contact changes, and therefore the breakdown of linearity in the particles' trajectories. We have verified that a plot with γ_0/p on the x-axis produces significantly worse collapse, and also that reducing the system size shifts the crossover to higher strains.

3.5. Relaxation and non-affine particle motion

When jammed solids are sheared, particles primarily slide past their contacting neighbors, rather than interpenetrating.[35, 63, 70, 88] This "floppy-like" motion is a precursor of true floppy modes, or zero frequency, non-rigid body eigenmodes, that appear below the jamming transition. Floppy-like motion is the physical origin of non-affine fluctuations. During floppy-like motion, relative displacements are predominantly perpendicular to the bond vector $\hat{\mathrm{r}}_{ij}$ pointing from the center of particle i to the center of particle j, not parallel to it. Floppy and non-affine motion is well understood in linear elastic response.[3, 63] However, little is known about how these displacements evolve in time, and/or in nonlinear response. Here we study the time evolution of the relative velocity of contacting particles during linear and nonlinear stress relaxation.

In order to analyze particle motions during relaxation, it is convenient decompose each relative velocity v_{ij} into longitudinal and transverse parts

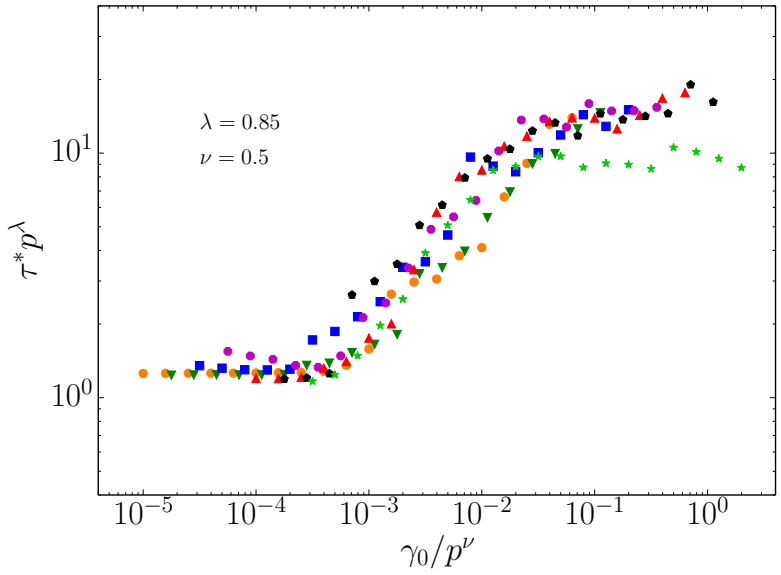

Figure 3.4: Data collapse of the relaxation time. Data are identical to Fig. 3.3.

according to

$$\mathbf{v}_{ij} = v_{\parallel,ij}\,\hat{\mathbf{r}}_{ij} + v_{\perp,ij}\,\hat{\mathbf{t}}_{ij}, \tag{3.5}$$

where the longitudinal velocity $v_\parallel$ is parallel to the $\hat{\mathbf{r}}_{ij}$ direction, and the transverse velocity $v_\perp$ isalong $\hat{\mathbf{t}}_{ij} = \hat{\mathbf{r}}_{ij} \times \hat{z}$, defined with respect to the unit vector $\hat{z}$ pointing out of the plane. By construction the particles have zero velocity at $t = 0$, and they approach a new static state at long times. During the relaxation process we follow the full statistics of the longitudinal and transverse velocities.

Fig. 3.5 shows the probability distribution functions (PDF's) of $|v_\parallel|$ and $|v_\perp|$ for one pressure $p = 10^{-3}$ and several times, presented in units of the relaxation time τ^* (see legend). For both longitudinal and transverse velocities, the distribution grows as $PDF \sim v$ for small v. The tails at large v are approximately exponential for short times $t/\tau^* \ll 1$. At longer times the distributions decay slower than an exponential and faster than a power law. Attempts to fit a stretched exponential do not yield a good fit. Rescaling velocities by their average value $\langle v_{\parallel,\perp} \rangle$ at each time provides an approximate collapse for times $t > \tau^*$, although some scatter remains. Due to this rough collapse, in the remainder we focus on average quantities, namely on the root mean squared (rms) velocities $v_\parallel^{\rm rms} \equiv \langle v_\parallel^2 \rangle^{1/2}$ and $v_\perp^{\rm rms} \equiv \langle v_\perp^2 \rangle^{1/2}$.

A representative example of the time evolution of the rms velocities is plotted in Fig. 3.6 for pressure $p = 10^{-3}$ and strain $\gamma_0 = 10^{-4}$, averaged over

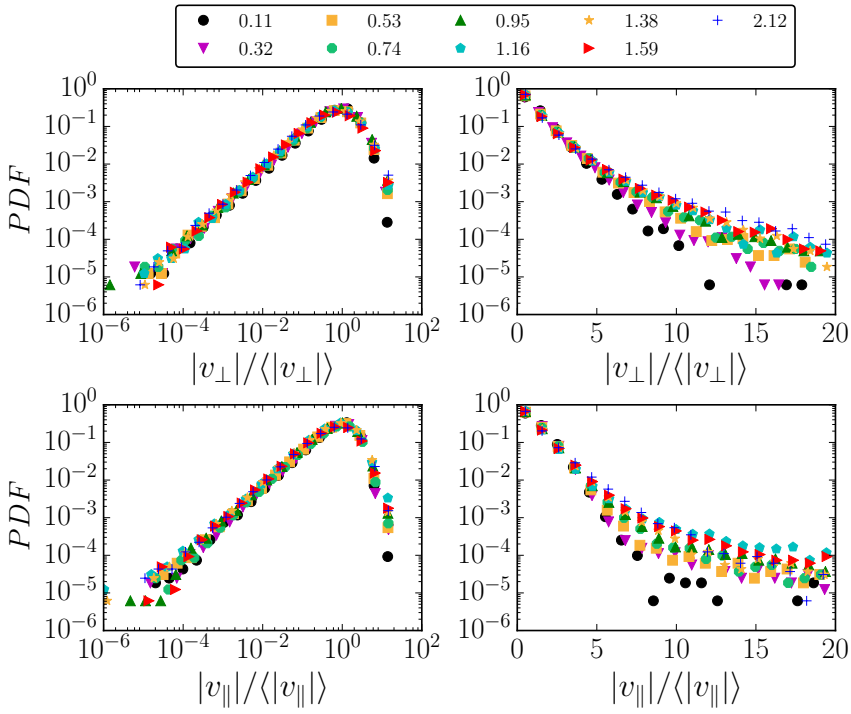

Figure 3.5: PDF's of longitudinal and transverse relative velocities at different times t/τ^* (see legend) in log-log and semi-log representations at $p = 10^{-3}$ and $\gamma_0 = 10^{-4}$.

an ensemble of 100 packings. Note that $v_\perp$ is substantially larger than $v_\parallel$ at all times, indicating that transverse motion is always dominant. After reaching their peak value at a time on the order of τ_0, the velocities steadily decrease as the packing relaxes, until eventually they drop sharply and simultaneously due to a fraction of the packings that fully arrest. This drop occurs long after the relaxation time, which is of the order $\tau^* \sim O(10^3)$ for this value of p and γ_0. Our interest here is primarily in the relaxation time τ^*, so in the remainder we focus on data at times prior to the drop.

To further assess the character of the particle motions at finite time, we introduce the ratio of rms velocities

$$\Gamma = \sqrt{\frac{\langle v_\perp^2 \rangle}{\langle v_\parallel^2 \rangle}}\,. \tag{3.6}$$

Γ measures the balance between motion that leads to sliding versus interpenetration. The value of Γ is of order unity for an affine velocity profile, while significantly larger values of Γ indicate strongly non-affine motion. In the following, we demonstrate that the relaxation of $1/\Gamma$ is strongly correlated with the relaxation of bulk stresses.

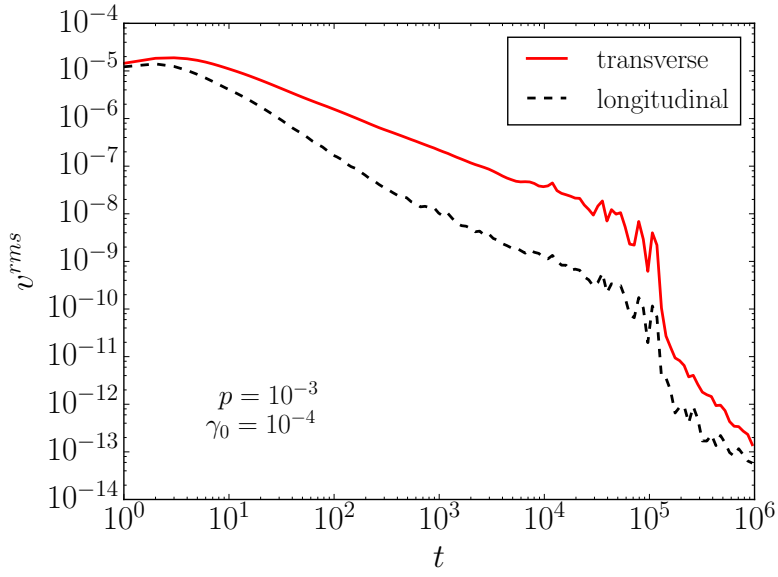

Figure 3.6: Longitudinal and transverse velocities versus time for $p = 10^{-3}$ and $\gamma_0 = 10^{-4}$.

Fig. 3.7 depicts $1/\Gamma$ for three values of the pressure and three values of the shear strain, for time intervals $10^{-3} \leq t/\tau^* \leq 10$. In all cases $1/\Gamma$ decays, indicating that non-affinity increases with time. For further comparison, we overplot the corresponding G_r in each panel (dashed lines). There is an evident similarity in their decay profiles; this strongly suggests a correlation between the mechanical relaxation time τ^* and the relaxation of floppy-like, non-affine fluctuations.

In order to further probe the correlation between stress relaxation and non-affine fluctuations, we investigate the time evolution of $1/\Gamma$ for three pressures and two values of the strain amplitude, as shown in Fig. 3.8. The first strain amplitude, $\gamma_0 = 10^{-6}$, is in the linear regime for all values of p, while the second, $\gamma_0 = 4 \times 10^{-3}$, is in the second plateau of τ^* in Fig. 3.4. For both low and high strain amplitudes, we find reasonable data collapse when time is rescaled by τ^* and Γ is rescaled with $p^{0.4}$. This data collapse is further evidence that the same physics governs the relaxation of non-affine fluctuations and stress, in both the linear and nonlinear regimes.

The data of Figs. 3.7 and 3.8 indicate a strong correlation between non-affinity at the micro scale, and stress response on the macro scale. They establish a microscopic interpretation of the relaxation time: it is the time scale beyond which floppy-like sliding motion (and hence non-affinity) fully dominates particle motion.

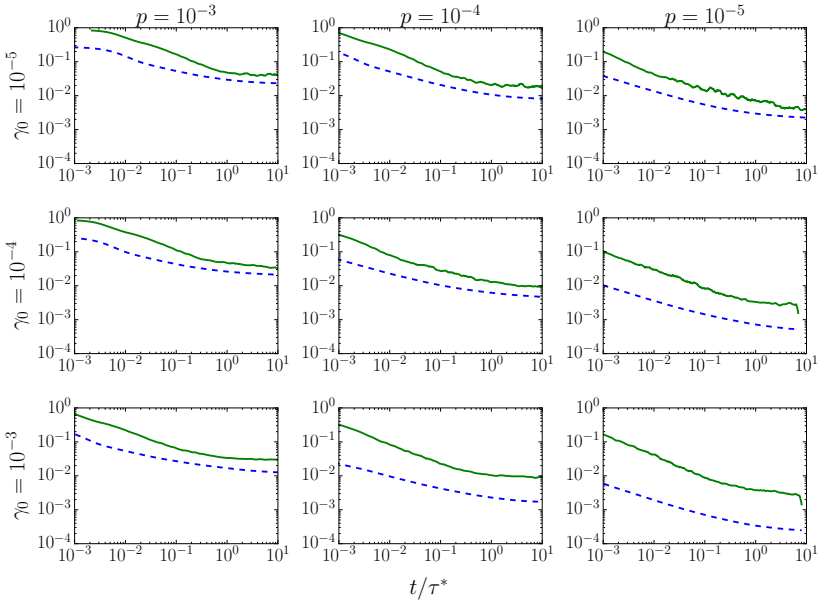

Figure 3.7: A comparison of the shear relaxation modulus G_r (dashed curves) with $1/\Gamma$ (solid curves) at three distinct pressures and strain amplitudes (see row and column labels).

3.6. Conclusion

We have used stress relaxation tests to determine the relaxation time of jammed solids as a function of strain and pressure. For sufficiently low strains, linear response is valid and the relaxation time approaches a plateau determined solely by the pressure. Close to jamming, the strains needed to access linear response are extremely small, and many experimental protocols are likely to probe nonlinear response even if care is taken to apply small strain. Beyond linear response, contact changes accumulate leading to softening, and the relaxation time grows. We find a second plateau in which τ^* is approximately independent of strain. To within the precision of our numerical measurement, this second plateau diverges at jamming with the same exponent that characterizes linear response. The crossover is associated with the onset contact changes, and hence the post-crossover plateau should be accessible experimentally. Rheometry and simultaneous particle tracking in bubble rafts[77, 99, 100] could also access measures of non-affinity.

In order to relate τ^* to microscopic properties of the system, we have studied the statistics of floppy-like, non-affine motion, characterized by the time-dependent ratio Γ of the rms longitudinal and transverse velocities between particles in contact. We observe a strong correlation between

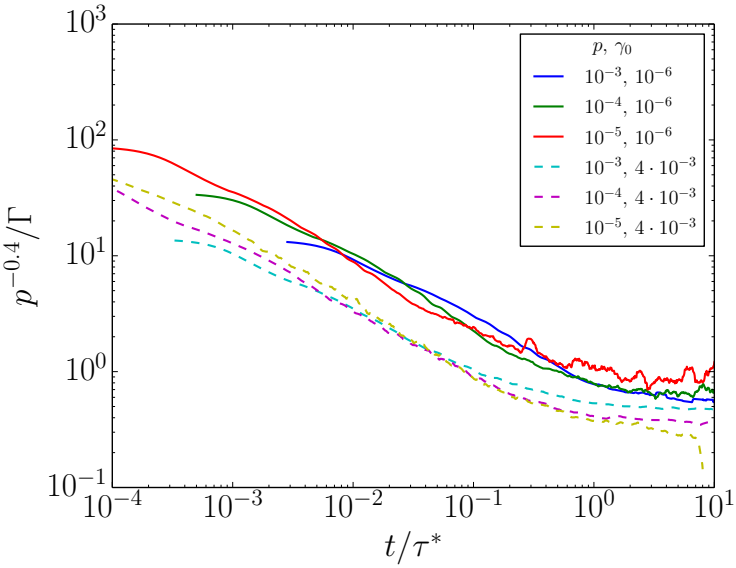

Figure 3.8: $p^{0.4}/\Gamma$ plotted as a function of the rescaled time coordinate t/τ^*. Solid and dashed curves are for (γ_0, p) pairs corresponding respectively to the linear and nonlinear plateaus of τ^* in Fig. 3.4.

Γ and the relaxation of shear stress in time. We infer that τ^* can be understood as the time needed to observe fully-developed non-affine response; once non-affinity has reached its maximum, the system's subsequent response is quasistatic.

There are several likely directions for future work. A natural question is whether the observed behavior of the relaxation time persists in $D = 3$ spatial dimensions. $D = 2$ is the upper critical dimension for the jamming transition [54, 69], so we do not anticipate qualitative differences. One can also ask how the relaxation time develops for larger strains, up to and including the yielding crossover to steady plastic flow, which occurs for strains on the order of 10%.[92] We speculate that there exists some strain scale beyond which the instantaneously applied step strain is tantamount to thermalization of the system, hence it may be possible to make connections to the late stages of relaxation after a temperature quench.[32] Finally, it is also interesting to ask if there is any relationship between the relaxation time studied here and the duration of rearrangement events in steady plastic flow.[101, 102]

4

Jamming and Irreversibility

We investigate irreversibility in soft frictionless disk packings on approach to the unjamming transition. Using simulations of shear reversal tests, we study the relationship between plastic work and irreversible rearrangements of the contact network. Infinitesimal strains are reversible, while any finite strain generates plastic work and contact changes in a sufficiently large packing. The number of irreversible contact changes grows with strain, and the stress-strain curve displays a crossover from linear to increasingly nonlinear response when the fraction of irreversible contact changes approaches unity.

This chapter is based on the following publication: J. Boschan, S. Luding, B.P. Tighe, Jamming and irreversibility, Granular Mat- ter, 21, 58, (2019).

Packings of soft spheres prepared at small but finite pressure are marginal solids – while their response to infinitesimal strains is elastic [4], a small shear stress suffices to instigate quasistatic plastic flow [25, 103]. Recently there has been considerable interest in how the ensemble- averaged stress-strain curve for shear becomes nonlinear, and in particular on how the crossover from linear to nonlinear response depends on the distance to jamming [33, 34, 41, 89, 92, 94, 104–107]. The shear strain required to make or break a contact vanishes in the limit of large system sizes, so finite deformations necessarily involve topological changes to the contact network [45, 47, 52, 91, 108]. It is therefore natural to ask about the relationship between nonlinearity and plasticity, especially when one approaches (un)jamming. More precisely, we ask whether there is a correlation between the linear-to-nonlinear crossover and (ir)reversibile contact changes.

To probe nonlinearity and irreversibility near jamming, we study shear reversal in marginally jammed packings of athermal, frictionless, purely repulsive soft spheres. We begin from an isotropic state prepared at a targeted pressure p. We use this initial pressure (prior to shearing) to quantify the distance to unjamming at $p = 0$. After preparation, the system is subjected to simple shear in small quasistatic steps to a maximum strain γ_m. The shearing direction is then reversed, and the system is returned to zero strain. A load is reversible if the stress follows the loading curve back to its initial value at zero strain. Reversible and irreversible deformations are illustrated in Fig. 4.1 with data from our simulations. This complements similar irreversibility under volumetric strain as observed in [105] and interpreted in terms of a history-dependent critical packing fraction.

The present work builds on results from Boschan et al. [92, 109], who studied the loading curve but did not consider shear reversal. The loading curve was found to be linear up to a strain scale $\gamma^\dagger \sim p$. After $\gamma^\dagger$ the stress continues to grow, albeit more slowly than an extrapolation of the initial linear trend. The crossover to steady plastic flow occurs later, at a distinct strain scale $\gamma_y \simeq 0.05$. Simulations of large amplitude oscillatory shear at finite rate also showed two distinct crossovers with identical scaling properties [106].

Boschan et al. [92] also studied contact changes, i.e. made and broken contacts during shearing. They found that the linear-to-nonlinear crossover at $\gamma^\dagger$ is also evident in the contact change statistics, as detailed in Section 4.3. It is plausible that contact changes are a proxy for irreversible rearrangements, but this must be verified – while rearrangements involve contact changes, not all rearrangements are irreversible [39, 40, 106, 110–113].

Here we probe nonlinearity and and irreversibility during a loading-unloading cycle. We first monitor the plastic work performed during the cycle, and then correlate these results to the statistics of contact changes

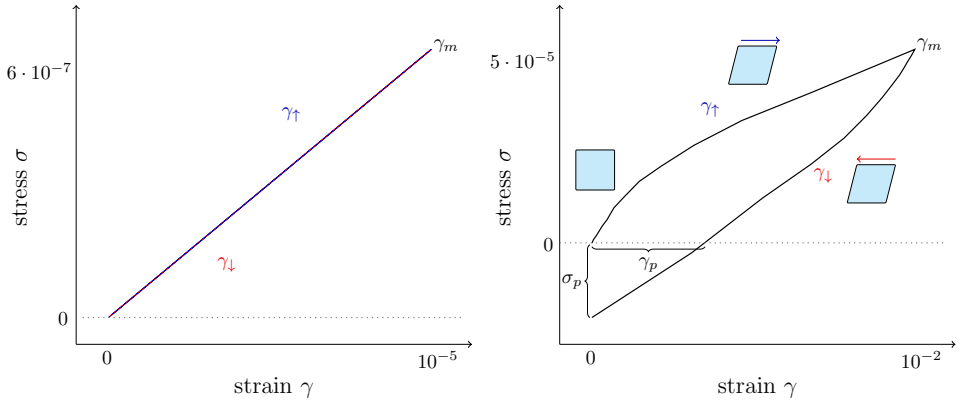

(a) Reversal straining in elastic case.

(b) Reversal straining in plastic case.

Figure 4.1: Sample output from a loading-unloading cycle in simulations. (a) If deformation is reversible, the loading curve $\sigma(\gamma_\uparrow)$ and unloading curve $\sigma(\gamma_\downarrow)$ coincide. (b) In an irreversible deformation there is hysteresis, and the enclosed area is equal to the plastic work.

at the particle scale. We find, first, that there is finite plastic work even when the ensemble-averaged stress-strain curve is linear. Consistent with this observation, we also find that irreversible contact changes accrue prior to the loss of linearity. Second, prior to $\gamma^\dagger$, some fraction of the contact changes are reversible. After $\gamma^\dagger$, when the stress-strain curve is nonlinear, essentially all contact changes are plastic.

4.1. Model and Methods

We perform two-dimensional simulations of athermal frictionless disks, a standard model with a jamming transition [30]. Particles experience a spring-like force proportional to their overlap $\delta_{ij} = (R_i + R_j) - r_{ij}$, where R_i and R_j denote the radii and r_{ij} is the length of the vector $\vec{r}_{ij}$ pointing from the center of particle i to j. The contact force on particle i due to particle j is purely repulsive, and there is no interaction when the particles are not in contact,

$$\vec{f}_{ij}^{\,\text{el}} = \begin{cases} -k(\delta_{ij})\delta_{ij}\hat{\vec{r}}_{ij} & \delta_{ij} \geq 0 \\ \vec{0} & \delta_{ij} < 0 \end{cases} \tag{4.1}$$

where a hat indicates a unit vector. We fix the units of stress by setting the spring constant k and mean particle size to unity. The stress tensor is

$$\sigma_{\alpha\beta} = -\frac{1}{2V} \sum_{ij} \mathrm{f}_{ij,\alpha} \mathrm{r}_{ij,\beta}, \tag{4.2}$$

where Greek indices denote Cartesian coordinates, and V is the total area of the unit cell.

Initial conditions are created by randomly populating the bi-periodic simulation box and then using a nonlinear conjugate gradient energy minimization protocol to quench instantaneously to a local minimum of the elastic potential energy at fixed volume [6]. The box is then allowed to undergo small changes in size and shape to achieve a target pressure p and zero shear stress – these are called "shear-stabilized" packings in the nomenclature of Dagois-Bohy et al. [54, 60]. Packings are bidisperse to avoid crystallization; we use the standard [4, 6] 50:50 mixture of small and large particles and a radius ratio of 1:1.4.

Once the initial state is prepared, we apply quasistatic simple shear using Lees-Edwards boundary conditions with small logarithmically-spaced steps ranging between $\Delta\gamma = 10^{-8} \ldots 10^{-3}$. After each strain step the energy is re-minimized [6] while holding the strain fixed, so particles follow quasistatic trajectories. Once a maximum strain γ_m is reached, the direction of shear is reversed and the system is returned to zero strain, again via a series of small logarithmically-spaced steps.

In order to quantify irreversibility, we calculate the plastic work W_p of the loading/unloading cycle,

$$W_p = \oint \sigma \, \mathrm{d}\gamma = \int_0^{\gamma_m} \sigma_\uparrow \, \mathrm{d}\gamma_\uparrow - \int_0^{\gamma_m} \sigma_\downarrow \, \mathrm{d}\gamma_\downarrow \,, \tag{4.3}$$

where upwards and downwards pointing arrows are used to indicate the loading and unloading curves, respectively. Clearly W_p is zero when the response is reversible.

The phenomenology of a shear reversal test in weakly jammed soft spheres is illustrated in Fig. 4.1. In panel (a), the maximum shear strain $\gamma_m = 10^{-5}$ is so small that no contact changes occur [52, 91]. The stress-strain curve is linear and the loading and unloading curves coincide. In panel (b), the maximum shear strain $\gamma_m = 10^{-2}$ is substantially larger. On reversal the stress decreases but does not retrace the loading curve. The loading and unloading curves are both nonlinear. Because there is hysteresis, there is an associated plastic work. In addition to the plastic work, irreversibility can be quantified by the plastic strain γ_p and a plastic stress σ_p, corresponding to the intercepts of the unloading curve with the x- and y-axis, respectively.

4.2. Plastic Work

We perform shear reversal tests for a range of preparation pressures p and varying maximum strain γ_m. Fig. 4.2 illustrates loading and unloading curves for $p = 10^{-4}$ and γ_m ranging from 10^{-5} to 10^{-2} in half-decade steps. The result is representative of other pressures.

To quantify the appearance of irreversibility, we analyze the plastic work as a function of γ_m and p, as shown in Fig. 4.3. We find nonzero W_p for all investigated maximum strains, which are as small as 10^{-5}. (As

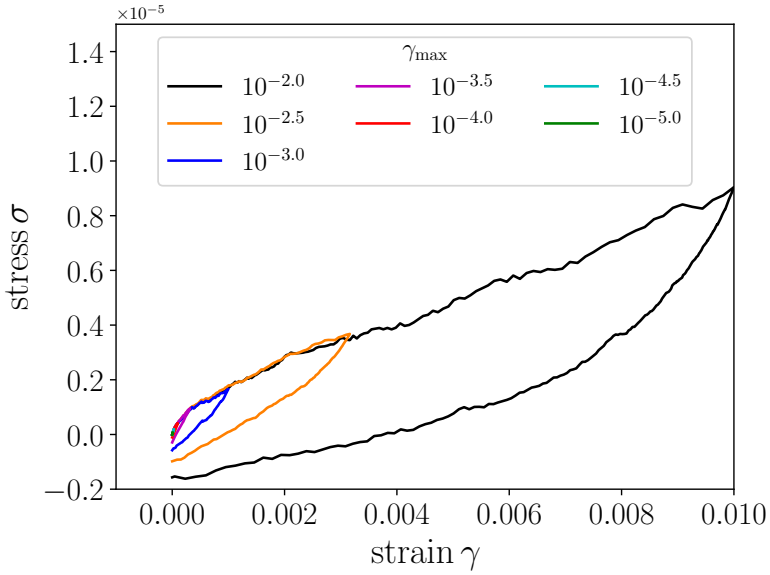

Figure 4.2: Shear reversal tests for varying maximum strains γ_m (see legend) at pressure $p = 10^{-4}$ and system size $N = 1024$.

noted above, packings of finite size can be sheared reversibly if the contact network remains unchanged, but this strain interval vanishes in the large system size limit [52, 91].) For each pressure W_p has an approximately power law growth with γ_m, with an apparent exponent that varies with pressure.

To better understand the pressure dependence of W_p, we seek to collapse the data to a master curve. Anticipating a correlation with the onset of nonlinearity, we plot the rescaled variable $x \equiv \gamma_m/p \sim \gamma_m/\gamma^\dagger$. On the other axis we plot the rescaled work $W \equiv W_p/p^\varrho$ for some exponent ϱ. To motivate ϱ, we note that for small values of γ_m, the loading curve is associated with work $W_\uparrow \sim G_0\gamma_m^2$, where $G_0 \sim p^{1/2}$ is the shear modulus for Hookean particles near jamming [4, 14, 35]. If we assume G_0 also sets the relevant scale for W_p at small γ_m, then we expect $W_p \sim p^{1/2}\gamma_m^2$. Rearranging in favor of γ_m/p gives $W_p/p^{5/2} \sim (\gamma_m/p)^2$, which requires $\varrho = 5/2$. This prediction is tested in the log-log plot of Fig. 4.3b, where we find data collapse to a curve with an initial slope of 2. When $x \gg x^* \sim O(1)$ the plastic work grows more slowly with γ_m, with an exponent of roughly $3/2$,

$$W \sim \begin{cases} x^2 & x < x^* \\ x^{3/2} & x > x^* \,. \end{cases} \tag{4.4}$$

Plasticity is indeed sensitive to $\gamma^\dagger$, because data for W_p collapse with the rescaled variable x. But irreversibility does not "turn on" when the

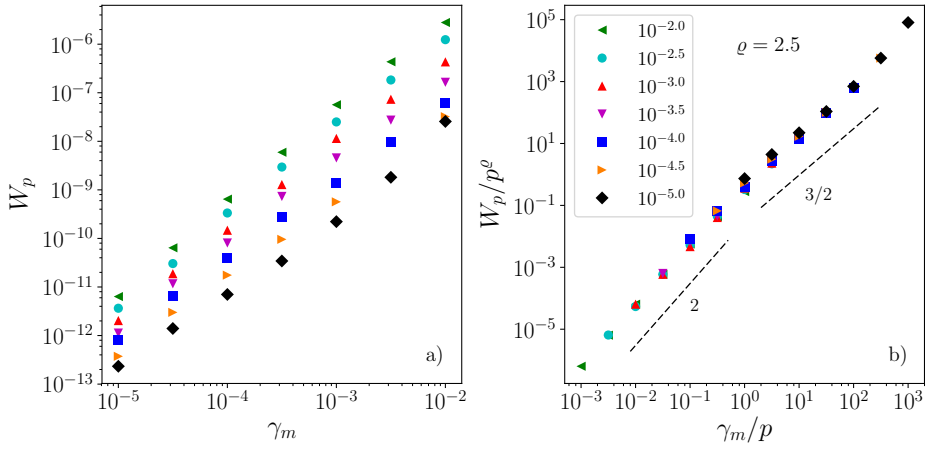

Figure 4.3: a) Plastic work versus maximum strain for varying pressures (see legend). b) Collapse to a master curve with $\varrho = 5/2$. The dashed lines have slopes 2 and $3/2$

ensemble-averaged stress-strain curve becomes nonlinear, as indicated by measurable W_p even when the curve is linear.

4.3. Contact changes

We now seek to relate irreversibility to the evolution of contact changes during loading and unloading.

As first shown in Ref. [92] and verified below, the scale $\gamma^\dagger$ is apparent in the evolution of the number of made and broken contacts per particle, which we refer to as the contact change density $n_{cc}(\gamma)$. We now monitor contact changes during unloading to see to what extent the original contact network is recovered (i.e. broken contacts are re-made and made contacts are re-broken). Contact changes are always identified with respect to the initial condition, even during unloading. The "plastic contact change density" n_{cc}^p, equal to n_{cc} at the end of the unloading curve, is a measure of irreversible (i.e. plastic) contact changes.

Fig. 4.4 depicts loading and unloading curves for three values of γ_m and three different initial pressures $p = 10^{-5}, 10^{-4}$ and 10^{-3}. For the lowest γ_m, in panel (a), most contact changes are recovered at the end of the cycle and n_{cc} has a nonzero slope. n_{cc}^p is nevertheless nonzero, and it increases as p tends to zero. Plastic contact changes also increase with increasing γ_m (panels (b) and (c)). In the final panel a large fraction of the contact changes are unrecoverable, n_{cc} hits the vertical axis with zero slope, and n_{cc}^p is nearly equal to $n_{cc}(\gamma_m)$.

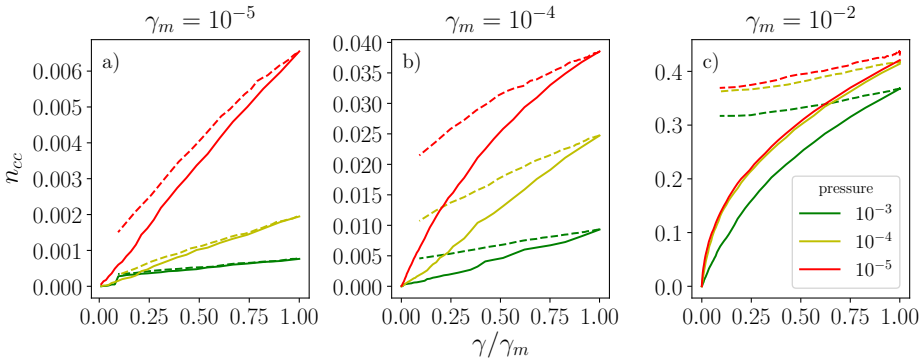

Figure 4.4: The contact change density n_{cc} as a function of γ/γ_m for a) $\gamma_m = 10^{-5}$, b) $\gamma_m = 10^{-4}$ and c) $\gamma_m = 10^{-2}$ each at pressures $p = 10^{-5}, 10^{-4}$ and 10^{-3} at $N = 1024$. The solid lines indicate the loading the dashed lines the unloading curves.

4

4.3.1. Contact changes during loading

Fig. 4.5 depicts n_{cc} during loading. The figure shows that data for different pressures can be collapsed to a master curve by plotting $N \equiv n_{cc}/(\gamma^\dagger)^{1/2} \sim n_{cc}/p^{1/2}$ as a function of $y = \gamma/p \sim \gamma/\gamma^\dagger$. This collapse was first demonstrated in Ref. [92]; for completeness we present it in Fig. 4.5 using data from the present study. We find

$$N \sim \begin{cases} y & y < y^* \\ y^{1/2} & y > y^* \,. \end{cases} \tag{4.5}$$

The crossover $y^* \sim O(1)$ is compatible with x^* from the plastic work. For later reference, we note that

$$n_{cc} \simeq a_m \gamma_m^{1/2} \tag{4.6}$$

when $\gamma_m > \gamma^\dagger = y^* p$. We estimate $a_m \approx 3.7 \pm 0.1$ by fitting Eq. (4.6) to N for $y > 10$.

We note that, by definition, n_{cc} changes by an amount $1/N$ when the system has undergone a strain γ_{cc} sufficient to produce one contact change. Hence

$$\frac{\mathrm{d}n_{cc}}{\mathrm{d}\gamma} \approx \frac{1/N}{\gamma_{cc}} \,, \tag{4.7}$$

and the average strain interval between contact changes, γ_{cc} can be read off from the slope of the curves in Fig. 4.4. (Alternatively, the probability of a contact change in the interval $[\gamma, \gamma + \mathrm{d}\gamma)$ is $1/\gamma_{cc}$.) In particular, when the loading curve is linear, there is a typical strain interval $\gamma_{cc} \sim p^{1/2}/N$ between contact changes. Van Deen et al. [52, 91] reached compatible results by directly resolving contact changes. As noted above, γ_{cc} vanishes in the large system size limit.

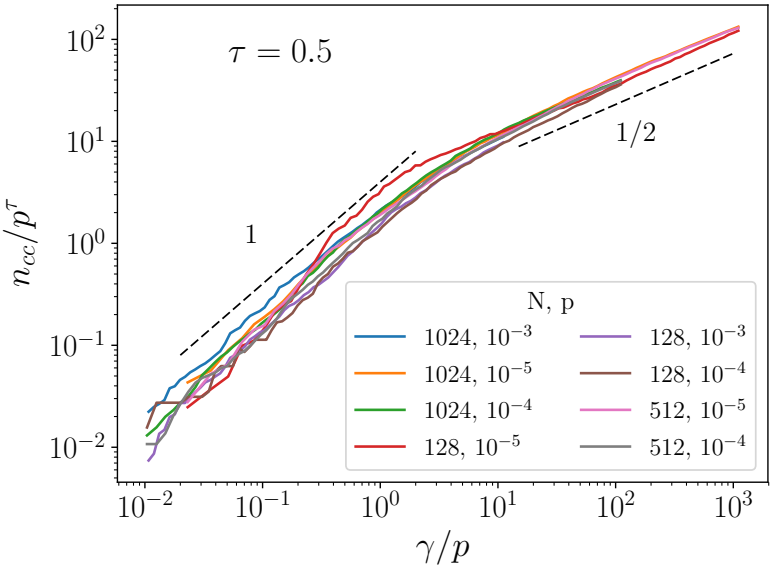

Figure 4.5: When appropriately rescaled with the pressure, the contact change density n_{cc} collapses to a master curve when plotted as a function of γ/p.

4.3.2. Contact changes after reversal

To quantify to what extent the initial contact network can be recovered under reversal, we now monitor the plastic contact change density n^p_{cc}. Clearly $n^p_{cc} = 0$ if the initial contact network is fully recovered. Fig. 4.6 plots n^p_{cc} as a function of γ_m for three pressures and system sizes $N = 128$, 512, and 1024. We find n^p_{cc} is an increasing function of γ_m, and for a given γ_m it is larger at smaller pressures. There is also dependence on N.

The system size-dependence in n^p_{cc} suggests that the contact change strain $\gamma_{cc} \sim p^{1/2}/N$ plays a dominant role, as opposed to $\gamma^\dagger \sim p$. To test this hypothesis, we attempt to collapse data to a master curve by plotting as a function of $z \equiv \gamma_m N/p^{1/2} \sim \gamma_m/\gamma_{cc}$. We find collapse plotting $P \equiv n^p_{cc} N^{1/2}/p^{1/4}$ versus $p^{1/2}/N$, as shown in Fig. 4.6b. The master curve is

$$P \sim \begin{cases} z & z < z^* \\ z^{1/2} & z > z^* \,. \end{cases} \tag{4.8}$$

The crossover value $z^* \sim O(10^2)$. Therefore

$$n^p_{cc} \simeq a_p \gamma_m^{1/2} \tag{4.9}$$

after the system has undergone on the order of one hundred contact changes. The constant $a_p \approx 3.5 \pm 0.1$.

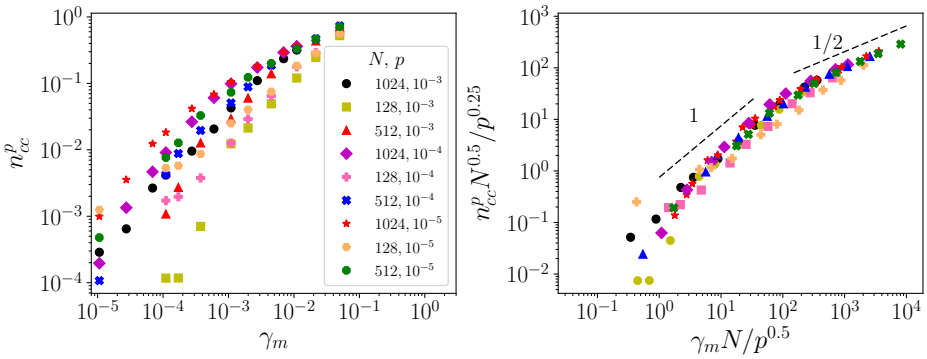

Figure 4.6: a) The plastic contact change density n_{cc}^p as a function of maximum strain γ_m at varying pressures p and system sizes N. b) Data collapse to a master curve. Dashed lines indicate the slopes 1 and 1/2.

4

4.3.3. Relating nonlinearity and irreversibility

We can use the above observations to interpret the strain scale $\gamma^\dagger$ in terms of irreversibility. To this end, it is useful to introduce the "plastic fraction"

$$f_p(\gamma_m) = \frac{\mathrm{d}n_{cc}^p}{\mathrm{d}n_{cc}^m}\,, \tag{4.10}$$

where n_{cc}^m is the value of n_{cc} at the end of loading. f_p quantifies the extent to which marginal contact changes tend to be plastic. If $f_p(\gamma_m) = 0$, then all marginal contact changes in an infinitesimal interval around γ_m are reversible. If $f_p = 1$, all contact changes are plastic.

While a direct numerical evaluation of f_p is noisy, we can infer its scaling properties by noting that

$$f_p = \left(\frac{\mathrm{d}n_{cc}^p}{\mathrm{d}\gamma_m}\right)\left(\frac{\mathrm{d}n_{cc}^m}{\mathrm{d}\gamma_m}\right)^{-1}. \tag{4.11}$$

From Eq. (4.9) it follows that

$$\frac{\mathrm{d}n_{cc}^p}{\mathrm{d}\gamma_m} \simeq \frac{a_p}{\gamma_m^{1/2}} \tag{4.12}$$

in the $N \to \infty$ limit. Similarly, Eq. (4.6) implies that

$$\frac{\mathrm{d}n_{cc}^m}{\mathrm{d}\gamma_m} \simeq \frac{a_m}{\gamma_m^{1/2}} \tag{4.13}$$

when $\gamma_m > \gamma^\dagger$. Thus f_p plateaus at a value $a_p/a_m \approx 0.95$ when $\gamma_m > \gamma^\dagger$. In other words, after the linear-to-nonlinear crossover, around 95% of the subsequent contact changes are plastic. By contrast, for smaller values of γ_m the plastic fraction evolves with strain.

4.3.4. From contact changes to the stress-strain curve

A remaining challenge is to determine how plastic events impact stress buildup. Here we make a first attempt. We expect irreversible contact changes to have an associated stress drop $\Delta\sigma_p/N$ due to an eigenvalue of the Hessian matrix going to zero [17, 114]. Then we assume that the infinitesimal stress $\mathrm{d}\sigma$ generated by a strain $\mathrm{d}\gamma$ has both an elastic contribution and an offsetting stress release due to irreversible events

$$\mathrm{d}\sigma = G_0\,\mathrm{d}\gamma - \Delta\sigma_p\,\mathrm{d}n^p_{cc}(\gamma)\,. \tag{4.14}$$

Using Eq. (4.9) and rewriting in dimensionless form gives

$$\frac{1}{G_0}\frac{\mathrm{d}\sigma}{\mathrm{d}\gamma} = 1 - \frac{\Delta\sigma_p}{p^{1/2}\,G_0}\left(\frac{p}{\gamma}\right)^{1/2}\,. \tag{4.15}$$

It remains to determine the typical stress drop amplitude, $\Delta\sigma_p$. The scaling relation $\Delta\sigma_p \sim p$ suggests itself purely on dimensional grounds. Assuming this form then predicts that the right hand side of Eq. (4.15) depends on γ and p only via their ratio γ/p. Reassuringly, this is consistent with the linear-to-nonlinear crossover at $\gamma^\dagger \sim p$, and with recent measurements of the secant modulus during shear startup [92] and the storage modulus in oscillatory shear [34, 106]. We conclude that the typical stress drop is indeed linear in p. Eq. (4.15) can then be integrated to find

$$\sigma \sim \begin{cases} p^{1/2}\,\gamma & \gamma < \gamma^\dagger \\ p\,\gamma^{1/2} & \gamma > \gamma^\dagger\,. \end{cases} \tag{4.16}$$

This stress-strain curve is compatible with W_p in Fig. 3b, including the $\gamma^{3/2}$ scaling beyond $\gamma \approx \gamma^\dagger$.

The approach presented above is semi-empirical. A more fundamental motivation would require directly identifying plastic events to determine their frequency and associated stress drops. The necessary theoretical tools were recently developed in Refs. [95, 114, 115].

4.4. Discussion

We have investigated irreversibility at the macro and micro scale in systems near jamming, evidencing irreversibility in both the plastic work and the contact change statistics for small shear strains. Initially the average loading curve is linear and most contact changes are reversible. Increasing the maximum strain increases the number and fraction of plastic contact changes. For $\gamma > \gamma^\dagger$, the loading curve becomes nonlinear and nearly all contact changes are plastic. The onset of nonlinearity therefore corresponds not to the *onset* of irreversibility (as commonly assumed in continuum elasto-plastic theories), but to "fully developed" irreversibility, as reflected in the saturation of the plastic fraction f_p. This crossover occurs earlier for smaller $\gamma^\dagger \sim p$.

With hindsight, the above scenario is apparent in the contact change statistics. For small γ_m, as in Fig. 4.4(a), the plastic contact change density is much smaller than n_{cc}^m, and the unloading branch of the n_{cc} curve ends with a nonzero slope – indicating that shearing the system "a little bit further" to $\gamma_\downarrow < 0$ would bring the system closer to its initial contact topology, i.e. fewer net contact changes. In contrast, for large γ_m, as in Fig. 4.4c, n_{cc}^p is nearly equal to n_{cc}^m, and the unloading curve is flat – the system has effectively lost all memory of its initial condition.

Our work has correlated the onset of nonlinearity at the macro scale to a particle scale crossover from reversible to irreversible contact changes. Both of these crossovers are sensitive to the proximity to jamming. We have also suggested a phenomenological approach to relate irreversible rearrangements to the form of the loading curve, highlighting the need for a deeper understanding of the statistics of stress drops during loading.

5

Conclusions and Outlook

In this thesis we focused on linear stress-strain response in disordered athermal solids, close to the jamming transition ($p_c = 0$). We discussed linearity in terms of Hooke's law, where the ratio of stress σ and strain γ is a constant, the shear modulus $G = \sigma/\gamma$. We did different type of simulations to investigate the validity of linear response in soft sphere packings. By combining macroscopic properties with investigation of changes in the contact network topology, we described how and why linear response breaks.

There are two ways for linear elasticity to break down: one, shearing 'too far' and two shearing 'too fast'. This thesis explored these two effects and their causes. We showed that together they set the boundaries to linear response and as (un)jamming is approached, the boundaries become narrower. In the following we will discuss our results in more detail.

Shearing 'too far': When a solid is strained it builds up stress to withstand the deformation. How well it can do that is captured by its shear modulus. In Ch. 2 we performed step strain simulations of soft sphere packings to describe the stress-strain relationship in the nonlinear regime. We have shown that for small strains the shear modulus is indeed constant, but when pushed too far, the material softens and the shear modulus decreases. A characteristic strain scale determines the crossover from linear to nonlinear response. Our simulations showed that the characteristic strain is proportional to the pressure for the system:

$$\gamma^\dagger \sim p.$$

This shows that close the transition, the smallest deformation can break linear response. One might expect that the onset of nonlinearity corresponds with irreversibility in the stress-strain curve. In Ch. 4 we measured irreversibility on a macro and micro scale by applying strain in one direction and reversing to zero strain. Afterwards the initial and final states were compared. We found that even for small deformations the plastic work is nonzero and it steadily increases with the maximum strain applied. While the plastic work is sensitive to $\gamma^\dagger$, there is measurable plastic dissipation prior to the onset of softening.

To complete the picture we examined the system on the micro scale. We related softening to changes in the contact network, by asking how many contact changes are needed until linear response breaks. In Ch. 2 we counted the number of made and broken contacts, at each applied strain, and concluded that an initially isotropic material softens This gives a topological criterion for the onset of softening.

In Ch. 4 we extended our conclusions about the contact network by measuring how much of it can be recovered after shear reversal. We found that the number of plastic (non-recoverable) contact changes grows with the maximum strain, until the initial contact network has been fully wiped out. We saw that softening is associated with this "saturation" of the plastic contact changes.

Shearing 'too fast': In viscoelastic materials deformations are followed by internal dynamics, which in time result in a return to mechanical equilibrium. The relaxation happens on a characteristic time scale, the relaxation time, τ^*. For deformations that are faster than τ^* viscous losses dominate the dynamics while they become negligible compared to elastic forces for deformations slower than τ^*. The relaxation time diverges at the jamming transition [35]. In Ch. 2 we performed flow start up tests, to measure the dependence of linear response on strain rate $\dot{\gamma}$ and the distance to jamming. Hooke's law was recovered.

By systematically varying the strain rate, we identified three different regimes, dependent on strain rate. 1) For slow rates the response is quasistatic, right from the start. In that case viscous effects are vanishingly slow and linear response breaks, only when the material softens. 2) For higher rates we first see rate-dependence, which at characteristic strain $\gamma^* = \dot{\gamma}\tau^*$, crosses over to quasistatic linear response. 3) If the rate is increased even more, γ^* is higher than the characteristic strain scale for softening. The rate-dependent stress-strain curve misses quasistatic linear response entirely. We concluded that there is no strain window over which Hooke's law holds when the system is sheared faster than a certain strain rate:

$$\dot{\gamma}^\dagger \sim p^2.$$

In many experiments finite strain rates are applied. Our scaling arguments provide important guidelines for setup and interpretation of such experiments.

We have seen that the relaxation time controls the appearance of rate-dependent effects, and that rate-dependent and nonlinear effects interact. Therefore in Ch. 3 we performed stress relaxation tests, systematically varying step strain size and the distance to jamming. When plotting the relaxation time as a function of strain amplitude, we found two plateaus, where the relaxation time was roughly constant. Both plateaus scale with the distance to jamming. This is an important result, as the relaxation time connected to linear response is likley to be inaccessible in experiments. Experimental strain rates are likely to probe the second regime.

From investigations done on the micro scale we saw that the relaxation is due to non-affine motions of the particles. We interpret the relaxation time as the time needed for the system to fully develop non-affine response.

References

[1] PTWIZ, *Arrow created by PTWIZ,* thenounproject.com/term/doodle-arrow/2405560.

[2] A. J. Liu and S. R. Nagel, *Nonlinear dynamics: Jamming is not just cool any more,* Nature **396**, 21 (1998).

[3] M. Wyart, S. R. Nagel, and T. A. Witten, *Geometric origin of excess low-frequency vibrational modes in weakly connected amorphous solids,* EPL **72**, 486 (2005).

[4] C. S. O'Hern, L. E. Silbert, A. J. Liu, and S. R. Nagel, *Jamming at zero temperature and zero applied stress: The epitome of disorder,* Phys. Rev. E **68**, 011306 (2003).

[5] D. Vågberg, P. Olsson, and S. Teitel, *Glassiness, rigidity, and jamming of frictionless soft core disks,* Phys. Rev. E **83**, 031307 (2011).

[6] D. J. Koeze, D. Vågberg, B. B. T. Tjoa, and B. P. Tighe, *Mapping the jamming transition of bidisperse mixtures,* EPL **113**, 54001 (2016).

[7] D. J. Durian, *Foam mechanics at the bubble scale,* Phys. Rev. Lett. **75**, 4780 (1995).

[8] H. M. Jaeger and A. J. Liu, *Far-from-equilibrium physics: An overview,* (2010).

[9] J. C. Maxwell, *L. on the calculation of the equilibrium and stiffness of frames,* The London, Edinburgh, and Dublin Philosophical Magazine and Journal of Science **27**, 294 (1864).

[10] A. Baule, F. Morone, H. J. Herrmann, and H. A. Makse, *Edwards statistical mechanics for jammed granular matter,* Rev. Mod. Phys. **90**, 015006 (2018).

[11] C. S. O'Hern, S. A. Langer, A. J. Liu, and S. R. Nagel, *Random packings of frictionless particles,* Phys. Rev. Lett. **88**, 075507 (2002).

[12] L. D. Landau and E. M. Lifshitz, *Theory of Elasticity* (Butterworth-Heineman, Oxford, 1997).

[13] G. Mase, *Schaum's Outline of Continuum Mechanics*, Schaum's outline of theory and problems (McGraw-Hill Education, 1970).

[14] M. Wyart, *On the rigidity of amorphous solids,* Annales de Physique **30**, 1 (2005).

[15] J. H. Aubert, A. M. Kraynik, and P. B. Rand, *Aqueous foams,* Scientific American **254**, 74 (1986).

[16] D. J. Durian, D. A. Weitz, and D. J. Pine, *Scaling behavior in shaving cream,* Phys. Rev. A **44**, R7902 (1991).

[17] C. E. Maloney and A. Lemaître, *Amorphous systems in athermal, quasistatic shear,* Phys. Rev. E **74**, 016118 (2006).

[18] M. Miner, *Arrow created by Max Miner,* thenounproject.com/term/hand-drawn-arrow/2440601.

[19] D. J. Durian, *Bubble-scale model of foam mechanics:mmelting, nonlinear behavior, and avalanches,* Phys. Rev. E **55**, 1739 (1997).

[20] A. W. Lees and S. F. Edwards, *The computer study of transport processes under extreme conditions,* Journal of Physics C: Solid State Physics **5**, 1921 (1972).

[21] D. Frenkel and B. Smit, *Understanding Molecular Simulation*, 2nd ed. (Academic Press, Inc., Orlando, FL, USA, 2001).

[22] E. Bitzek, P. Koskinen, F. Gähler, M. Moseler, and P. Gumbsch, *Structural relaxation made simple,* Phys. Rev. Lett. **97**, 170201 (2006).

[23] H. A. Barnes and J. F. Hutton, *An Introduction to Rheology* (Elsevier, 1989).

[24] F. Bolton and D. Weaire, *Rigidity loss transition in a disordered 2d froth,* Phys. Rev. Lett. **65**, 3449 (1990).

[25] B. P. Tighe, E. Woldhuis, J. J. C. Remmers, W. van Saarloos, and M. van Hecke, *Model for the scaling of stresses and fluctuations in flows near jamming,* Phys. Rev. Lett. **105**, 088303 (2010).

[26] G. Katgert, B. P. Tighe, and M. van Hecke, *The jamming perspective on wet foams,* Soft Matter **9**, 9739 (2013).

[27] T. Hatano, *Growing length and time scales in a suspension of athermal particles,* Phys. Rev. E **79**, 050301 (2009).

[28] J. R. Seth, L. Mohan, C. Locatelli-Champagne, M. Cloitre, and R. T. Bonnecaze, *A micromechanical model to predict the flow of soft particle glasses,* Nat Mater **10**, 838 (2011).

[29] S. V. Franklin and M. D. Schattuck, eds., *Handbook of Granular Materials* (CRC Press, 2015).

[30] M. van Hecke, *Jamming of soft particles: Geometry, mechanics, scaling and isostaticity,* J. Phys. Cond. Matt. **22**, 033101 (2010).

[31] A. J. Liu and S. R. Nagel, *The jamming transition and the marginally jammed solid,* Ann. Rev. Cond. Matt. Phys. **1**, 347 (2010).

[32] D. A. Head, *Critical scaling and aging in cooling systems near the jamming transition,* Phys. Rev. Lett. **102**, 138001 (2009).

[33] C. Coulais, A. Seguin, and O. Dauchot, *Shear modulus and dilatancy softening in granular packings above jamming,* Phys. Rev. Lett. **113**, 198001 (2014).

[34] M. Otsuki and H. Hayakawa, *Avalanche contribution to shear modulus of granular materials,* Phys. Rev. E **90**, 042202 (2014).

[35] B. P. Tighe, *Relaxations and rheology near jamming,* Phys. Rev. Lett. **107**, 158303 (2011).

[36] L. R. Gómez, A. M. Turner, M. van Hecke, and V. Vitelli, *Shocks near jamming,* Phys. Rev. Lett. **108**, 058001 (2012).

[37] S. Ulrich, N. Upadhyaya, B. van Opheusden, and V. Vitelli, *Shear shocks in fragile networks,* PNAS **110**, 20929 (2013).

[38] S. van den Wildenberg, R. van Loo, and M. van Hecke, *Shock waves in weakly compressed granular media,* Phys. Rev. Lett. **111**, 218003 (2013).

[39] M. Lundberg, K. Krishan, N. Xu, C. S. O'Hern, and M. Dennin, *Reversible plastic events in amorphous materials,* Phys. Rev. E **77**, 041505 (2008).

[40] I. Regev, R. Lookman, and C. Reichhardt, *Onset of irreversibility and chaos in amorphous solids under periodic shear,* Phys. Rev. E **88**, 062401 (2013).

[41] E. D. Knowlton, D. J. Pine, and L. Cipelletti, *A microscopic view of the yielding transition in concentrated emulsions,* Soft Matter **10**, 6931 (2014).

[42] N. C. Keim and P. E. Arratia, *Mechanical and microscopic properties of the reversible plastic regime in a 2d jammed material,* Phys. Rev. Lett. **112**, 028302 (2014).

[43] N. C. Keim and P. E. Arratia, *Role of disorder in finite-amplitude shear of a 2d jammed material,* Soft Matter **11**, 1539 (2015).

[44] T. Kawasaki, D. Coslovich, A. Ikeda, and L. Berthier, *Diverging viscosity and soft granular rheology in non-brownian suspensions,* Physical Review E **91**, 012203 (2015).

[45] G. Combe and J.-N. Roux, *Strain versus stress in a model granular material: A devil's staircase,* Phys. Rev. Lett. **85**, 3628 (2000).

[46] E. Lerner, G. Düring, and M. Wyart, *Low-energy non-linear excitations in sphere packings,* Soft Matter **9**, 8252 (2013).

[47] C. F. Schreck, T. Bertrand, C. S. O'Hern, and M. D. Shattuck, *Repulsive contact interactions make jammed particulate systems inherently nonharmonic,* Phys. Rev. Lett. **107**, 078301 (2011).

[48] C. F. Schreck, R. S. Hoy, M. D. Shattuck, and C. S. O'Hern, *Particle-scale reversibility in athermal particulate media below jamming,* Phys. Rev. E **88**, 052205 (2013).

[49] C. F. Schreck, C. S. O'Hern, and M. D. Shattuck, *Vibrations of jammed disk packings with hertzian interactions,* Granular Matter **16**, 209 (2014).

[50] T. Bertrand, C. F. Schreck, C. S. O'Hern, and M. D. Shattuck, *Hypocoordinated solids in particulate media,* Phys. Rev. E **89**, 062203 (2014).

[51] I. Agnolin and J.-N. Roux, *Internal states of model isotropic granular packings. iii. elastic properties,* Phys. Rev. E **76**, 061304 (2007).

[52] M. S. van Deen, J. Simon, Z. Zeravcic, S. Dagois-Bohy, B. P. Tighe, and M. van Hecke, *Contact changes near jamming,* Phys. Rev. E **90**, 020202 (2014).

[53] C. P. Goodrich, A. J. Liu, and S. R. Nagel, *Comment on "repulsive contact interactions make jammed particulate systems inherently nonharmonic",* Phys. Rev. Lett. **112**, 049801 (2014).

[54] C. P. Goodrich, S. Dagois-Bohy, B. P. Tighe, M. van Hecke, A. J. Liu, and S. R. Nagel, *Jamming in finite systems: Stability, anisotropy, fluctuations, and scaling,* Phys. Rev. E **90**, 022138 (2014).

[55] D. Nakayama, H. Yoshino, and F. Zamponi, *Protocol-dependent shear modulus of amorphous solids,* Journal of Statistical Mechanics: Theory and Experiment **2016**, 104001 (2016).

[56] S. Dagois-Bohy, E. Somfai, B. P. Tighe, and M. van Hecke, *Large amplitude oscillatory shear near jamming,* (in preparation) (2014).

[57] C. P. Goodrich, A. J. Liu, and S. R. Nagel, *The principle of independent bond-level response: Tuning by pruning to exploit disorder for global behavior,* Phys. Rev. Lett. **114**, 225501 (2015).

[58] D. J. Evans and G. Morriss, *Statistical Mechanics of Nonequilibrium Liquids* (Cambridge University Press, 2008).

[59] G. Katgert and M. van Hecke, *Jamming and geometry of two-dimensional foams,* EPL **92**, 34002 (2010).

[60] S. Dagois-Bohy, B. P. Tighe, J. Simon, S. Henkes, and M. van Hecke, *Soft-sphere packings at finite pressure but unstable to shear,* Phys. Rev. Lett. **109**, 095703 (2012).

[61] R. Ramírez, T. Pöschel, N. V. Brilliantov, and T. Schwager, *Coefficient of restitution of colliding viscoelastic spheres,* Phys. Rev. E **60**, 4465 (1999).

[62] H. P. Zhang and H. A. Makse, *Jamming transition in emulsions and granular materials,* Phys. Rev. E **72**, 011301 (2005).

[63] W. G. Ellenbroek, E. Somfai, M. van Hecke, and W. van Saarloos, *Critical scaling in linear response of frictionless granular packings near jamming,* Phys. Rev. Lett. **97**, 258001 (2006).

[64] A. Zaccone and E. Scossa-Romano, *Approximate analytical description of the nonaffine response of amorphous solids,* Phys. Rev. B **83**, 184205 (2011).

[65] L. E. Silbert, A. J. Liu, and S. R. Nagel, *Diverging length scales near the jamming transition,* Phys. Rev. Lett. **95**, 098301 (2005).

[66] A. Tanguy, J. P. Wittmer, F. Leonforte, and J.-L. Barrat, *Continuum limit of amorphous elastic bodies: A finite-size study of low-frequency harmonic vibrations,* Phys. Rev. B **66**, 174205 (2002).

[67] S. Alexander, *Amorphous solids: their structure, lattice dynamics and elasticity,* Phys. Rep **296**, 65 (1998).

[68] C. Maloney, *Correlations in the elastic response of dense random packings,* Phys. Rev. Lett. **97**, 035503 (2006).

[69] C. P. Goodrich, A. J. Liu, and S. R. Nagel, *Finite-size scaling at the jamming transition,* Phys. Rev. Lett. **109**, 095704 (2012).

[70] B. P. Tighe, *Dynamic critical response in damped random spring networks,* Phys. Rev. Lett. **109**, 168303 (2012).

[71] M. Sheinman, C. P. Broedersz, and F. C. MacKintosh, *Nonlinear effective-medium theory of disordered spring networks,* Phys. Rev. E **85**, 021801 (2012).

[72] C. Zhao, K. Tian, and N. Xu, *New jamming scenario: From marginal jamming to deep jamming,* Phys. Rev. Lett. **106**, 125503 (2011).

[73] K. W. Desmond, P. J. Young, D. Chen, and E. R. Weeks, *Experimental study of forces between quasi-two-dimensional emulsion droplets near jamming,* Soft Matter **9**, 3424 (2013).

[74] I. Jorjadze, L.-L. Pontani, and J. Brujic, *Microscopic approach to the nonlinear elasticity of compressed emulsions,* Phys. Rev. Lett. **110**, 048302 (2013).

[75] R. Höhler and S. Cohen-Addad, *Rheology of liquid foam,* J. Phys. Cond. Matt. **17**, R1041 (2005).

[76] M. Le Merrer, R. Lespiat, R. Hohler, and S. Cohen-Addad, *Linear and non-linear wall friction of wet foams,* Soft Matter **11**, 368 (2015).

[77] G. Katgert, M. E. Möbius, and M. van Hecke, *Rate dependence and role of disorder in linearly sheared two-dimensional foams,* Phys. Rev. Lett. **101**, 058301 (2008).

[78] S. Cohen-Addad, H. Hoballah, and R. Höhler, *Viscoelastic response of a coarsening foam,* Phys. Rev. E **57**, 6897 (1998).

[79] A. J. Liu, S. Ramaswamy, T. G. Mason, H. Gang, and D. A. Weitz, *Anomalous viscous loss in emulsions,* Phys. Rev. Lett. **76**, 3017 (1996).

[80] F. P. Bretherton, J. Fluid Mech. **10**, 166 (1961).

[81] P. Olsson and S. Teitel, *Critical scaling of shear viscosity at the jamming transition,* Phys. Rev. Lett. **99**, 178001 (2007).

[82] D. Vågberg, P. Olsson, and S. Teitel, *Dissipation and rheology of sheared soft-core frictionless disks below jamming,* Phys. Rev. Lett. **112**, 208303 (2014).

[83] N. C. Keim, J. D. Paulsen, and S. R. Nagel, *Multiple transient memories in sheared suspensions: Robustness, structure, and routes to plasticity,* Phys. Rev. E **88**, 032306 (2013).

[84] C. Heussinger and E. Frey, *Stiff polymers, foams, and fiber networks,* Phys. Rev. Lett. **96**, 017802 (2006).

[85] C. Heussinger and E. Frey, *Floppy modes and nonaffine deformations in random fiber networks,* Phys. Rev. Lett. **97**, 105501 (2006).

[86] C. P. Broedersz, X. Mao, T. C. Lubensky, and F. C. MacKintosh, *Criticality and isostaticity in fibre networks,* Nat. Phys. **7**, 983 (2011).

[87] M. Das, D. Quint, and J. Schwarz, *Redundancy and cooperativity in the mechanics of compositely crosslinked filamentous networks,* PloS One **7**, e35939 (2012).

[88] M. Wyart, H. Liang, A. Kabla, and L. Mahadevan, *Elasticity of floppy and stiff random networks,* Phys. Rev. Lett. **101**, 215501 (2008).

[89] B. P. Tighe, *Shear dilatancy in marginal solids,* Granular Matter **16**, 203 (2014).

[90] A. C. Pipkin, *Lectures on Viscoelasticity Theory* (Springer New York, 1986).

[91] M. S. van Deen, B. P. Tighe, and M. van Hecke, *Contact changes of sheared systems: Scaling, correlations, and mechanisms,* Phys. Rev. E **94**, 062905 (2016).

[92] J. Boschan, D. Vågberg, E. Somfai, and B. P. Tighe, *Beyond linear elasticity: Jammed solids at finite shear strain and rate,* Soft Matter **12**, 5450 (2016).

[93] S. Farhadi, A. Z. Zhu, and R. P. Behringer, *Stress relaxation for granular materials near jamming under cyclic compression,* Phys. Rev. Lett. **115**, 188001 (2015).

[94] D. Nakayama, H. Yoshino, and F. Zamponi, *Protocol-dependent shear modulus of amorphous solids,* Journal of Statistical Mechanics: Theory and Experiment **2016**, 104001 (2016).

[95] L. Gartner and E. Lerner, *Nonlinear plastic modes in disordered solids,* Phys. Rev. E **93**, 011001 (2016).

[96] I. Srivastava and T. S. Fisher, *Slow creep in soft granular packings,* Soft Matter **13**, 3411 (2017).

[97] K. Khakalo, K. Baumgarten, B. P. Tighe, and A. Puisto, *Coarsening and mechanics in the bubble model for wet foams,* Phys. Rev. E **98**, 012607 (2018).

[98] K. Baumgarten and B. P. Tighe, *Viscous forces and bulk viscoelasticity near jamming,* Soft Matter **13**, 8368 (2017).

[99] J. Lauridsen, M. Twardos, and M. Dennin, *Shear-induced stress relaxation in a two-dimensional wet foam,* Phys. Rev. Lett. **89**, 098303 (2002).

[100] M. E. Möbius, G. Katgert, and M. van Hecke, *Relaxation and flow in linearly sheared two-dimensional foams,* EPL (Europhysics Letters) **90**, 44003 (2010).

[101] S. Tewari, D. Schiemann, D. J. Durian, C. M. Knobler, S. A. Langer, and A. J. Liu, *Statistics of shear-induced rearrangements in a two-dimensional model foam,* Physical Review E **60**, 4385 (1999).

[102] I. K. Ono, S. Tewari, S. A. Langer, and A. J. Liu, *Velocity fluctuations in a steadily sheared model foam,* Physical review E **67**, 061503 (2003).

[103] C. Heussinger and J.-L. Barrat, *Jamming transition as probed by quasistatic shear flow,* Phys. Rev. Lett. **102**, 218303 (2009).

[104] C. P. Goodrich, A. J., and J. P. Sethna, *Scaling ansatz for the jamming transition,* PNAS **113**, 9745 (2016).

[105] N. Kumar and S. Luding, *Memory of jamming–multiscale models for soft and granular matter,* Granular Matter **18**, 58 (2016).

[106] S. Dagois-Bohy, E. Somfai, B. P. Tighe, and M. van Hecke, *Softening and yielding of soft glassy materials,* Soft Matter **13**, 9036 (2017).

[107] K. Baumgarten and B. P. Tighe, *Normal stresses, contraction, and stiffening in sheared elastic networks,* Phys. Rev. Lett. **120**, 148004 (2018).

[108] N. Kumar, S. Luding, and V. Magnanimo, *Macroscopic model with anisotropy based on micro–macro information,* Acta Mechanica **225**, 2319 (2014).

[109] J. Boschan, S. A. Vasudevan, P. E. Boukany, E. Somfai, and B. P. Tighe, *Stress relaxation in viscous soft spheres,* Soft Matter **13**, 6870 (2017).

[110] K. Saitoh, V. Magnanimo, and S. Luding, *A master equation for the probability distribution functions of forces in soft particle packings,* Soft Matter **11**, 1253 (2015).

[111] I. Regev, J. Weber, C. Reichhardt, K. A. Dahmen, and T. Lookman, *Reversibility and criticality in amorphous solids,* Nature Communications **6**, 8805 (2015).

[112] N. V. Priezjev, *Reversible plastic events during oscillatory deformation of amorphous solids,* Phys. Rev. E **93**, 013001 (2016).

[113] K. Saitoh, N. Oyama, F. Ogushi, and S. Luding, *Transition rates for slip-avalanches in soft athermal disks under quasi-static simple shear deformations,* Soft matter (2019).

[114] M. S. van Deen, *Mechanical response of foams: elasticity, plasticity, and rearrangements*, Ph.D. thesis (2016).

[115] E. Lerner, *Micromechanics of nonlinear plastic modes,* Phys. Rev. E **93**, 053004 (2016).

Curriculum Vitæ

Júlia BOSCHÁN

28-11-1987 Born in Budapest, Hungary.

Education

2007–1999	Grammar School Gymnasium, Münster (1999–2005) Budapest, Hungary (2005–2007)
2008–2011	BSc. in Physics Roland Eötvös University, Budapest
2011–2013	MSc. in Nuclear Engieneering Swiss Federal Polytechnic School (ETH), Zürich

List of Publications

3. **J. Boschan, S. Luding, B.P. Tighe**, *Jamming and irreversibility*, Granular Matter, **21**, 58, (2019).

2. **J. Boschan, S.A. Vasudevan, P.E. Boukany, E. Somfai, B.P. Tighe**, *Stress relaxation in viscous soft spheres*, Soft Matter, **13**, 6870-6876, (2017).

1. **J. Boschan, D. Vågberg, E. Somfai, B.P. Tighe**, *Beyond linear elasticity: jammed solids at finite shear strain and rate* , Soft Matter, **12**, 5450-5460,(2016).

Acknowledgements

I would like to thank Brian, my co-promoter and daily supervisor for all the work we did together. Thank you for the support in getting started as a researcher, teaching and guiding me. I learned valuable lessons from you about patience when chasing results and how to successfully communicate and present them.

My Promoter Thijs, for the opportunity to teach and to blow-up a barrel of ping-pong balls on a regular basis. Thank you for your encouragement and support while pushing me towards the finish line.

Thank you Ellák for all your cooperation and help with numerical matters, sharing your code and talks when I was visiting Hungary. Daniel, thank you for sharing your code for quasistatic simulations and introducing me to the finer parts of soft matter simulations.

I also want to thank Stefan Luding for his cooperation and particularly his input in the last paper (Chapter 4).

As a PhD student you are part of a great community of colleagues and often friends, who support and challenge you. I want to thank all who made it possible. Dion, I appreciate the creative ideas we shared and fondly remember our never ending discussions about simulations, foams, the Netherlands, the world and everything else. Remco, you have encouraged me to write and helped put my thoughts in order, thank you for becoming a friend I can always turn to. Sebastián, I can always count on your sane opinion which I appreciate so much and thank you for making the office so much more fun. Mariëtte, you were the one who showed the ropes when I started. I thank you for always listening, giving me advice and perspective. Thank you also Metin, Tim, Merlijn, Christos, Mahinder, Hassan, Vilborg, Dennis, Sarah, Selin, Marilena and Ana.

This is also a great occasion to thank my family, who have encouraged me and without whom this would have not been possible. My husband Árpi, you always believe I can do anything I set my mind to. This means so much to me, thank you. My incredible parents, Peter and Eva, who were the greatest role models. You taught me, how to be happy and achieve what I want in life. My sisters, Kati and Viki, I have learned so much from you and gone this far also because of the a way you paved for me. My friends who are family, Katti and Lilla. I thank you knowing me as much as you do and supporting me no matter what. For me the greatest joy is my family and I am super happy to also know the support of extended family. Thank you Irénke, Gábor, Marci, Dan, Lexi and Marco.